OPEN ACCESS

Original research

Targeting cancer-associated fibroblast-secreted WNT2 restores dendritic cell-mediated antitumour immunity

Tu-Xiong Huang,[1,2] Xiang-Yu Tan,[1] Hui-Si Huang,[1] Yu-Ting Li,[1] Bei-Lei Liu,[3] Kai-Sheng Liu,[2] Xinchun Chen,[1] Zhe Chen,[4] Xin-Yuan Guan,[3] Chang Zou,[2] Li Fu [1]

► Additional material is published online only. To view, please visit the journal online (http://dx.doi.org/10.1136/gutjnl-2020-322924).

[1]Guangdong Provincial Key Laboratory of Regional Immunity and Diseases, Department of Pharmacology and International Cancer Center, Shenzhen University Health Science Center, Shenzhen, China
[2]Shenzhen People's Hospital, The Second Clinical Medical College of Jinan University, The First Affiliated Hospital of Southern University of Science and Technology, Shenzhen, China
[3]Department of Clinical Oncology, The University of Hong Kong, Hong Kong, China
[4]Key Laboratory of Digestive Pathophysiology of Zhejiang Province, First Affiliated Hospital, Zhejiang Chinese Medical University, Hangzhou, China

Correspondence to
Professor Li Fu, Pharmacology, Shenzhen University, Shenzhen, Guangdong, China;
gracelfu@szu.edu.cn

T-XH and X-YT are joint first authors.

Received 26 August 2020
Revised 22 February 2021
Accepted 24 February 2021
Published Online First
10 March 2021

To cite: Huang T-X, Tan X-Y, Huang H-S, *et al*. *Gut* 2022;**71**:333–344.

ABSTRACT

Objective Solid tumours respond poorly to immune checkpoint inhibitor (ICI) therapies. One major therapeutic obstacle is the immunosuppressive tumour microenvironment (TME). Cancer-associated fibroblasts (CAFs) are a key component of the TME and negatively regulate antitumour T-cell response. Here, we aimed to uncover the mechanism underlying CAFs-mediated tumour immune evasion and to develop novel therapeutic strategies targeting CAFs for enhancing ICI efficacy in oesophageal squamous cell carcinoma (OSCC) and colorectal cancer (CRC).

Design Anti-WNT2 monoclonal antibody (mAb) was used to treat immunocompetent C57BL/6 mice bearing subcutaneously grafted mEC25 or CMT93 alone or combined with anti-programmed cell death protein 1 (PD-1), and the antitumour efficiency and immune response were assessed. CAFs-induced suppression of dendritic cell (DC)-differentiation and DC-mediated antitumour immunity were analysed by interfering with CAFs-derived WNT2, either by anti-WNT2 mAb or with short hairpin RNA-mediated knockdown. The molecular mechanism underlying CAFs-induced DC suppression was further explored by RNA-sequencing and western blot analyses.

Results A negative correlation between $WNT2^+$ CAFs and active $CD8^+$ T cells was detected in primary OSCC tumours. Anti-WNT2 mAb significantly restored antitumour T-cell responses within tumours and enhanced the efficacy of anti-PD-1 by increasing active DC in both mouse OSCC and CRC syngeneic tumour models. Directly interfering with CAFs-derived WNT2 restored DC differentiation and DC-mediated antitumour T-cell responses. Mechanistic analyses further demonstrated that CAFs-secreted WNT2 suppresses the DC-mediated antitumour T-cell response via the SOCS3/p-JAK2/p-STAT3 signalling cascades.

Conclusions CAFs could suppress antitumour immunity through WNT2 secretion. Targeting WNT2 might enhance the ICI efficacy and represent a new anticancer immunotherapy.

Significance of this study

What is already known on this subject?

- Immunomodulatory interactions between tumour cells and the immunosuppressive tumour microenvironment (TME) skew the positive response to immunotherapy in solid tumours.
- Cancer-associated fibroblasts (CAFs) are an abundant and critical component of the TME and negatively regulate antitumour immunity.
- CAFs-secreted WNT2 has a critical role in the malignant progression of oesophageal squamous cell carcinoma (OSCC) and colorectal cancer (CRC). Further exploration of the role of CAFs-derived WNT2 in regulating antitumour immunity is merited.

What are the new findings?

- The density of $WNT2^+$ CAFs is negatively correlates with the percentage of active $CD8^+$ T cells in primary OSCC tumours.
- An anti-WNT2 monoclonal antibody (mAb) newly developed in our group significantly enhances the therapeutic efficacy of anti-programmed cell death protein 1 (PD-1) mAb by increasing active dendritic cells (DCs) in both OSCC and CRC allograft tumours and improves the tumour-killing activity of splenic T cells.
- Directly targeting CAF-derived WNT2 restores DC differentiation and DC-mediated antitumour T-cell responses both in vitro and in vivo.
- CAFs-secreted WNT2 suppresses the DC-mediated antitumour T-cell response via the SOCS3/p-JAK2/p-STAT3 signalling cascades.

How might it impact on clinical practice in the foreseeable future?

- Our findings open up a new therapeutic strategy to enhance the efficacy of PD-1/programmed death-ligand 1 immune checkpoint treatment by targeting CAFs-secreted WNT2 or other CAFs-induced immunosuppressive factors, not only in OSCC and CRC but more broadly.

INTRODUCTION

Programmed cell death protein 1 (PD-1)/programmed death-ligand 1 (PD-L1) immune checkpoint inhibitors have shown encouraging results since they were approved in 2014 for treating various solid tumours and haematological malignancies.[1 2] Nevertheless, many patients with solid malignancies do not respond to PD-1/PD-L1 checkpoint inhibitor treatment.[3 4] The hindrance to achieving long-lasting therapeutic responses in solid tumours is, in part, mediated by the dynamic nature of these tumours and their complex microenvironment.[5] Cancer-associated fibroblasts (CAFs) are the

most abundant stromal cells in the tumour microenvironment (TME) and are thought to suppress antitumour immunity in a variety of solid tumours.[6–9] However, the mechanisms by which CAFs regulate antitumour immune responses in solid tumours remain unclear.

Our previous study identified FGFR2 as a specific marker of pro-tumourigenic CAFs in oesophageal squamous cell carcinoma (OSCC).[10] FGFR2$^+$ CAFs can secrete WNT2 and thus activate the Wnt/β-catenin signalling pathway to promote the malignant progression of OSCC.[11] WNT2 is a glycoprotein ligand secreted by the Wnt signalling pathway; it can initiate intracellular signalling and participates in different processes involved in the regulation of development.[12] WNT2 also promotes the malignant progression of other solid tumours, including colorectal cancer (CRC), gastric cancer (GC) and breast cancer (BC).[13–15] The expression pattern of WNT2 varies among different cancers. In OSCC and CRC, WNT2 is mainly expressed by CAFs rather than tumour cells,[11 13] but is expressed by both CAFs and tumour cells in BC[16] and GC.[17] WNT proteins also play an important role in the development of effector T cells, activation of regulatory T cells (Tregs), and dendritic cell (DC) differentiation and maturation.[18] It has been reported that the overexpression of Wnt5a can suppress the differentiation of plasma-like DCs and classical DCs through non-canonical Wnt signalling pathways.[19] The canonical Wnt/β-catenin pathway in DCs is also involved in the regulation of DC differentiation and migration.[20 21] Recent studies have shown that endogenous Wnt5a or β-catenin in melanoma cells can regulate immune-evasion by tumour cells via influencing the tumour infiltration or biological functions of DCs.[22 23] However, to the best of our knowledge, specific targeting of WNT5A and its downstream effectors for immunotherapy has not been reported yet.

CAFs-derived WNT2 is commonly expressed in GI cancers,[11 13 14] but its role in the regulation of antitumour immunity is still largely unknown. To date, most studies have focused on the development of combination immunotherapies by blocking different immune checkpoints of immune cells to enhance the efficacy of PD-L1/PD-1 blockade. New strategies by targeting CAFs-induced immunosuppressive signalling may provide an alternative for effective combination immunotherapies in solid tumours. In this study, we sought to investigate the role of CAFs-secreted WNT2 in regulating antitumour immunity and explore a new way to develop more efficient immunotherapies for patients with GI cancer with high expression of WNT2.

MATERIALS AND METHODS

Mice and in vivo treatments

Four to six-week-old female C57BL/6 mice were purchased from Charles River Laboratories (Beijing, China) and maintained under specific pathogen-free conditions. All animal procedures were performed in accordance with guidelines approved by the Institutional Animal Care and Use Committee at Shenzhen University Health and Science Center. mEC25 cells (4×10^6 cells/mouse) or CMT93 cells (1×10^6 cells/mouse) were subcutaneously injected into the right flanks of the mice. Mice were randomly assigned to treatment groups when they had developed tumours of about 5 mm in diameter. Mice were intraperitoneally injected every 3 days for 2 weeks with 200 μg control IgG (MOPC-21; Bio X cell), 200 μg anti-WNT2 (3C4; custom-made at Kexing Biotech, Hangzhou, China) and 10 mg/kg anti-PD-1 (29F.1A12; Bio X cell) or anti-WNT2 combined with anti-PD-1. The tumour volume was calculated using the formula: Volume=$\pi\times$length$\times$width$\times$height/6.

In vivo tumour growth assay

mEC25 cells (4×10^6 cells/mouse), combined with mCAF-shWnt2 (1.3×10^6 cells/mouse) or mCAF-shNTC (1.3×10^6 cells/mouse) cells were subcutaneously injected into the right flanks of the mice. The tumour volume was calculated using the formula: Volume=$\pi\times$length$\times$width$\times$height/6.

Flow cytometry analysis

For the in vitro DC differentiation analysis, mouse bone marrow DCs were generated, as previously described.[24] Briefly, bone marrow cells of C57BL/6 mice were cultured in RPMI 1640 medium containing 10% FBS with granulocyte/macrophage colony-stimulating factor (GM-CSF) (10 ng/mL)+interleukin (IL)-4 (10 ng/mL) for 7 days to induce the cells to differentiate into DCs. The culture medium (CM) from wild-type (WT) mCAFs, mCAF-shNTC or mCAF-shWnt2 was used to treat the cells during DC induction. In some experiments, WT CAF.CM was preincubated with control IgG (MOPC-21; 100 μg/mL) or anti-WNT2 (3C4; 100 μg/mL) before DC induction. The DCs were stained with fluorescein isothiocyanate (FITC)-conjugated anti-CD11c (HL3; BD PharMingen) and/or allophycocyanin (APC)-conjugated anti-IDO (mIDO-48; eBioscience) or anti-IL-10 (JES5-16E3; Biolegend), followed by flow cytometry analysis using the CytoFLEX system and Kaluza software (Beckman Coulter). To evaluate the activities of DCs after being cultured for 7 days, as described earlier, DCs were stimulated with lipopolysaccharide (LPS) (200 ng/mL; 24 hours) followed by counter-staining with FITC-conjugated anti-CD11c (HL3) and phycoerythrin (PE)-conjugated anti-TNFα (MP6-XT22; eBioscience), anti-IL12 (C17.8; eBioscience), anti-CD80 (16-10A1; eBioscience) or anti-CD86 m(GL1; eBioscience). DCs were also stimulated with mEC25 cell lysate (1:1; 12 hours), followed by coincubation with CD8$^+$ T cells for 5 days. The co-cultured cells were then stained with FITC-conjugated anti-CD8 (53–6.7; BD Biosciences) and APC-conjugated anti-interferon (IFN)-γ antibody (XMG1.2; eBioscience). For the analysis of mouse tumour-derived DCs or T cells, tumour tissues were cut into small pieces, digested with 1 mg/mL collagenase IV (Sigma), and homogenised through a 100 μm mesh filter. After washing, the isolated single cells were blocked with anti-CD16/32 (93; eBioscience), followed by staining with antibodies against CD11c+TNFα, CD11c+IL12, CD11c+CD80, CD11c+CD86 or CD8+IFN-γ. For the analysis of mouse splenic T cells, the spleen was cut into small pieces and homogenised through a 100 μm mesh filter. After washing, the cell pellet was resuspended in 40% Percoll (Sigma) and the lymphocytes were isolated according to the manufacturer's instructions. Splenic lymphocytes were blocked with anti-CD16/CD32 and counterstained with anti-CD8 and anti-IFN-γ, followed by flow cytometry analysis using the CytoFLEX system and Kaluza software (Beckman Coulter).

Additional methodology is provided as online supplemental information.

RESULTS

WNT2$^+$ CAFs negatively correlate with effector T cells in OSCC tumours

We first investigated whether there was a correlation between WNT2$^+$ CAFs and effector T cells within the TME. Our previous studies showed that FGFR2$^+$ CAFs could provide a suitable microenvironment for tumour development through WNT2 secretion.[10 11] Thus, WNT2$^+$FGFR2$^+$ CAFs were considered to be pro-tumourigenic CAFs, and their regulation of antitumour immunity was investigated in the present

study. Paraffin-embedded tumour sections from 47 primary OSCC cases were double immunostained with markers for pro-tumourigenic CAFs ($WNT2^+FGFR2^+$), Tregs ($Foxp3^+CD4^+$) and active $CD8^+$ T cells ($IFN\text{-}\gamma^+CD8^+$). The expression of $WNT2^+FGFR2^+$ CAFs, $Foxp3^+CD4^+$ Tregs and $IFN\text{-}\gamma^+CD8^+$ effector T cells was quantified and analysed by Tissue FAXSFluo. The number of $WNT2^+FGFR2^+$ CAFs was positively correlated with the ratio of $Foxp3^+CD4^+$ T cells/$CD4^+$ T cells (figure 1A) and negatively correlated with the ratio of $IFN\text{-}\gamma^+CD8^+$ T cells/$CD8^+$ T cells (figure 1B). OSCC cases with <37 $WNT2^+FGFR2^+$ CAFs per 1 mm^3 of tumour tissue were defined as low-$WNT2^+$ cases, while cases with ≥37 $WNT2^+FGFR2^+$ CAFs were defined as high-$WNT2^+$ cases. Compared with the ratio in low-$WNT2^+$ cases, high-$WNT2^+$ cases with a high density of $WNT2^+FGFR2^+$ CAFs had a higher ratio of $Foxp3^+CD4^+$ T cells/$CD4^+$ T cells (figure 1C,D) and a lower ratio of $IFN\text{-}\gamma^+CD8^+$ T cells/$CD8^+$ T cells (figure 1C,E) in the TME. These results indicate that $WNT2^+FGFR2^+$ CAFs might confer potent immunosuppressive effects in the oesophageal cancer microenvironment.

Anti-WNT2 monoclonal antibody treatment effectively enhances antitumour immunity in OSCC and CRC

To evaluate the potential of a $WNT2^+$ CAF-targeting strategy for enhancing antitumour responses, an anti-WNT2 monoclonal antibody (designated anti-WNT2) recently developed in our group was used alone or in combination with anti-PD-1 antibody to study its antitumour effects in syngeneic mouse OSCC and CRC models. The anti-WNT2 antibody used in this study was highly specific. It did not recognise other human WNT proteins (eg, WNT2B, WNT3A, WNT5A, WNT5B, WNT7B and WNT11), which have more than 40% homology with WNT2 (online supplemental figure 1A), but it was able to recognise both human WNT2 (hWNT2) (online supplemental figure 1A) and mouse Wnt2 (online supplemental figure 1B). Mice bearing syngeneic mEC25 tumours (figure 2A) or CMT93 tumours (online supplemental figure 2A) were treated with anti-WNT2 (200 µg/mouse) or/and anti-PD-1 (10 mg/kg/mouse) intraperitoneally every 3 days for five times. Anti-WNT2 treatment significantly suppressed the tumour growth in both OSCC (figure 2B,C) and CRC (online supplemental figure 2B,C) models. A combination of anti-WNT2 and anti-PD-1 produced more effective inhibition than anti-WNT2 or anti-PD-1 when they were used individually.

Antitumour T-cell responses were also measured in freshly resected tumours by flow cytometry. The ratio of $IFN\text{-}\gamma^+CD8^+$ T cells/$CD8^+$ T cells in mEC25 tumours (figure 2D) were enhanced by anti-WNT2 or anti-PD-1 treatment, compared with these values in the control. Combination treatment with anti-WNT2 and anti-PD-1 induced more activated $CD8^+$ T cells in tumours than individual treatment with anti-WNT2 or anti-PD-1. The enhanced T-cell responses within tumours induced by anti-WNT2 or/and anti-PD-1 treatment are consistent with their growth-suppressing effects. Anti-WNT2 treatment also effectively improved the tumour-killing activity of $CD8^+$ T cells in spleens obtained from mEC25 tumour-bearing mice (figure 2E), suggesting that anti-WNT2 may improve the initiation of adoptive antitumour immunity. DCs always play a critical role in initiation of tumour-killing T-cell responses.[25] To determine whether anti-WNT2 treatment has an impact on the immune-stimulating activity of DCs, the percentage of DCs and their maturation in mEC25 tumours were examined. The percentage of $CD11c^+$ DCs (figure 2F) or of $CD103^+$ DCs (figure 2G) was significantly enhanced in the anti-WNT2-treated tumours compared with the percentage in the control IgG-treated tumours. Additionally, the percentage of matured DCs ($CD80^+CD11c^+$ DCs and $CD86^+CD11c^+$ DCs) in tumours were enhanced by anti-WNT2 treatment (figure 2H,I). Similarly, anti-WNT2 treatment also enhanced antitumour T-cell responses (online supplemental figure 2D,E) and activated DCs (online supplemental figure 2F-I) in syngeneic mouse CRC model. Notably, although anti-PD-1 enhanced more activated $CD8^+$ T cells than anti-WNT2 in CMT93 tumours ($p=0.0481$; online supplemental figure 2D), it's improvement of systemic antitumour immunity in CMT93 tumour-bearing mice is significantly lower than that of anti-WNT2 ($p=0.0012$; online supplemental figure 2E), suggesting that anti-WNT2 may have advantages in improving initiation of adoptive antitumour immunity. These findings suggested that combination immunotherapy with anti-WNT2 and anti-PD-1 not only enhanced the systemic antitumour T-cell response but also restored the tumour-killing activity of tumour-derived $CD8^+$ T cells, which had been suppressed by PD-L1/PD-1 signalling within the TME. Notably, anti-WNT2 treatment showed its safety in mouse tumour model since anti-WNT2 preferred to bind to tumour area rather than normal tissues including heart, liver, spleen, lung and kidney (online supplemental figure 3A,B). Moreover, no significant histological changes were detected in the above normal vital organs by anti-WNT2 treatment (online supplemental figure 3C).

CAFs-secreted WNT2 suppresses the differentiation and immune-stimulating activities of DCs in vitro

To further explore the role of WNT2 in regulating DC-mediated antitumour T-cell responses, we investigated the ability of recombinant WNT2 to suppress DC differentiation and activation by flow cytometry analyses based on the gating strategy shown in online supplemental figure 4. Compared with the control results, recombinant mouse-Wnt2 protein (mWnt2) could effectively suppress the differentiation of mouse $CD11c^+$ DCs (online supplemental figure 5A) and $CD103^+$ DCs (online supplemental figure 5B) in vitro. Treatment with mWnt2 also inhibited the activated phenotypes ($TNF\alpha^+CD11c^+$ DCs and $IL12^+CD11c^+$ DCs; online supplemental figure 5C,D) and the matured phenotypes ($CD80^+CD11c^+$ DCs and $CD86^+CD11c^+$ DCs; online supplemental figure 5E,F) of DCs on simulation with LPS. WNT2 is therefore able to suppress DC differentiation and their activated phenotypes. Importantly, mWnt2 treatment suppressed the activity of $CD11c^+$ DCs for priming $CD8^+$ T cells when pulsed with tumour antigens (online supplemental figure 5G). Consistently, ELISA results showed that mWnt2 treatment could inhibit the secretion of TNFα and IL12 by DCs on LPS stimulation (online supplemental figure 5H1) and the secretion of IFN-γ by $CD8^+$ T cells which were primed by tumour antigen-loaded DCs (online supplemental figure 5J). Blockade with anti-WNT2 IgG or anti-WNT2 Fab significantly attenuated all immunosuppressive effects induced by the mWnt2 protein in vitro (online supplemental figure 5). Furthermore, we investigated whether hWNT2 protein possesses similar activity for suppressing DC function compared with that of mWnt2. Recombinant hWNT2 also suppressed the differentiation of DCs (online supplemental

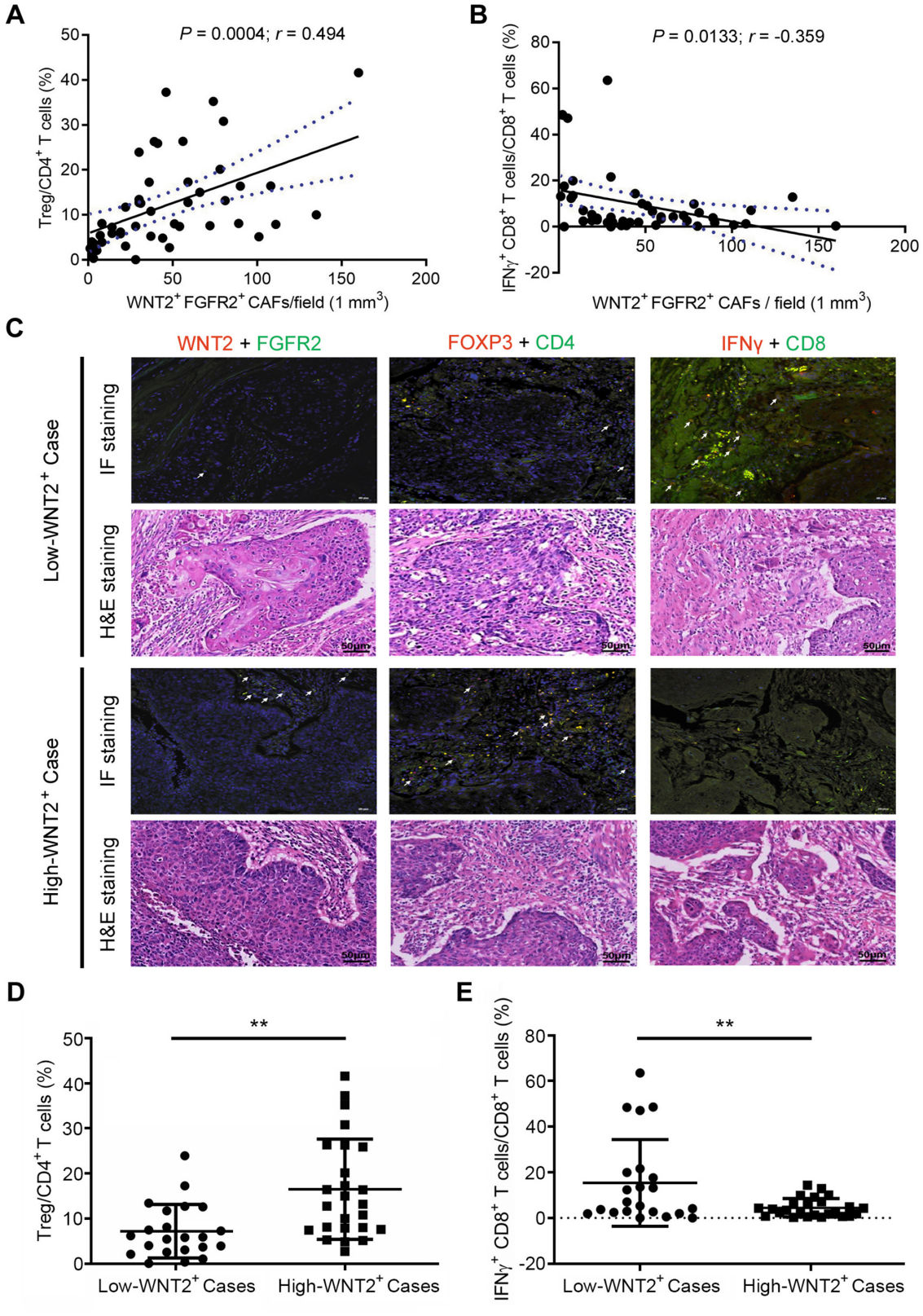

Figure 1 Correlation between WNT2$^+$ cancer-associated fibroblasts (CAFs) and T-cell immune-stimulating activities in patients with oesophageal squamous cell carcinoma (OSCC). (A) Positive correlation between the density of WNT2$^+$ CAFs and the ratio of Tregs/CD4$^+$ T cells in OSCC tissue sections (n=47), expressed using Pearson's correlation coefficient. The solid line shows the linear regression; dotted lines indicate the 95% CIs. (B) Negative correlation between the density of WNT2$^+$ CAFs and the ratio of interferon (IFN)-γ$^+$ CD8$^+$ T cells/CD8$^+$ T cells in OSCC tissue sections (n=47). (C) Representative immunofluorescence (IF) images of WNT2$^+$ CAFs, Tregs and effector CD8$^+$ T cells (upper) and their matched H&E images (lower) between low-WNT2 and high-WNT2$^+$ cases. Low-WNT2$^+$: <37 WNT2$^+$FGFR2$^+$ CAFs in 1 mm^3 tumour tissue; high-WNT2$^+$: ≥37 WNT2$^+$FGFR2$^+$ CAFs in 1 mm^3 tumour tissue. (D, E) The ratios of Tregs/CD4$^+$ T cells (D) or IFN-γ$^+$ CD8$^+$ T cells/CD8$^+$ T cells (E) between low-WNT2$^+$ and high-WNT2$^+$ cases were compared. The values are shown as means±SEM. **p<0.01, ****p<0.0001, using the Student's t-test.

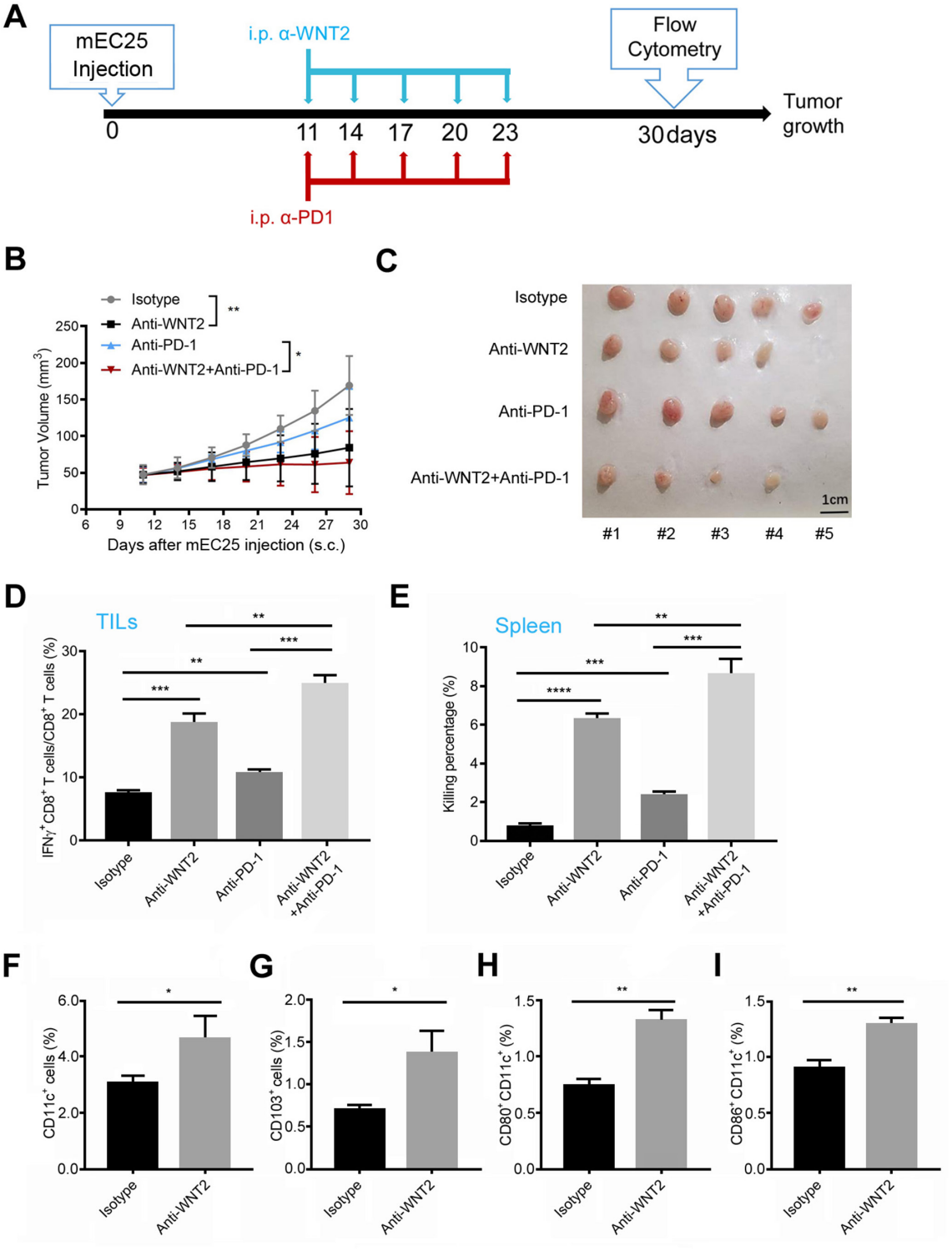

Figure 2 Anti-WNT2 therapy induced tumour-killing immunity and enhanced the therapeutic efficacy of anti-programmed cell death protein 1 (PD-1) in mouse oesophageal squamous cell carcinoma. (A) Schematic of the drug intervention protocol for α-WNT2 (intraperitoneally) and/or α-PD-1 (intraperitoneally) in C57BL/6 mice subcutaneously implanted with mEC25 cells. At the drug intervention end-point, mouse tissues were obtained for flow cytometry. (B) Average tumour growth curves of syngeneic mEC25 tumours in mice treated as described in (A). (C) The visual maps of mEC25 tumours by indicated treatment. The tumours were removed from mice at day 30 after mEC25 cell injection. (D) Flow cytometry was used to quantify the percentage of effective $CD8^+$ T cells (interferon (IFN)-γ^+) in anti-WNT2, anti-PD-1 and IgG isotype-treated mice (n=5/group). (E) A cytotoxic lymphocyte assay evaluated the tumour-killing activity of $CD8^+$ T cells isolated from mice spleens treated in (D). (F–I) Flow cytometry analysis was used to quantify the percentage of $CD11c^+$ dendriticcells (DCs) (F), $CD103^+$ DCs (G), $CD80^+CD11c^+$ DCs (H) and $CD86^+CD11c^+$ cells (I) in tumours from mice treated in (D). Data are shown as means±SEM. *p<0.05, **p<0.01, ***p<0.001, ****p<0.0001 by two-way analysis of variance (ANOVA) in (B) or Student's t-test in (D–I).

figure 6A,B) and the generation of their matured population (online supplemental figure 6C,D) while anti-WNT2 IgG or anti-WNT2 Fab significantly attenuated all immunosuppressive effects induced by the hWnt2 protein in vitro (online supplemental figure 6).

We next explored whether WNT2 mediates the regulation by CAFs of DC differentiation and function. Mouse FGFR2$^+$ CAFs (mCAFs) were isolated from primary mouse OSCC tumours which were established as previously[26]; WNT2 is primarily expressed and secreted by CAFs rather than tumour cells in mouse OSCC tumours (online supplemental figure 7A,B). The CM of mCAFs (mCAF.CM) was used to treat DC precursors, and the differentiation and immune-stimulating activity was measured. Similar to the mWnt2 protein treatment, mCAFs showed good activity for suppressing DC differentiation (figure 3A), enhancing CD11c$^+$ DC inhibitory phenotypes (figure 3B,C), and inhibiting DC maturation (figure 3D,E), activation (figure 3F) and priming CD8$^+$ T cells (figure 3G). Treating mCAF.CM with anti-WNT2 could significantly overcome all the immunosuppressive effects induced by mCAF.CM (figure 3), suggesting that WNT2 secretion is a critical mediator for the regulation of DC differentiation and functioning by CAFs.

Additionally, mCAFs were transfected with a lentivirus plasmid expressing control shRNA or Wnt2-targeting shRNA to construct mCAF-shNTC and mCAF-shWnt2, respectively (figure 4A,B). The mCAF-shNTC.CM showed similar activity to mCAF.CM, suppressing DC differentiation (figure 4C,D), activation (figure 4E) and maturation (figure 4F,G). The reduction in Wnt2 induced by specific shRNA significantly restored the differentiation and immune-stimulating activity of DCs (figure 4), showing a consistent trend with anti-WNT2 treatment. Taken together, either recombinant mWnt2/hWNT2 protein or mCAF.CM suppressed DC differentiation and function. Blocking WNT2 activities with anti-WNT2 or interfering *Wnt2* expression in CAFs with Wnt2-targeting shRNA could overcome these suppressions, indicating that CAF-secreted WNT2 may play a critical role in regulating DC differentiation and function.

Knockdown of *Wnt2* in mCAFs inhibits mEC25 tumour growth by enhancing the DC-mediated antitumour T-cell response

We further explored the role of CAFs-secreted WNT2 in regulating DC-mediated antitumour immunity within the TME of solid tumours in animal model. Importantly, in a syngeneic mouse tumour model established by subcutaneous injection of mEC25 cells and mCAFs (ratio: 3:1), the reduction in Wnt2 expression in mCAFs significantly attenuated their activity in promoting mEC25 tumour progression (figure 5A,B) and suppressing the activity of CD8$^+$ T cells (figure 5C). Compared with the results in the mCAF-shNTC+mEC25 group, the mCAF-shWnt2+mEC25 group had more CD8$^+$ T cells producing IFN-γ (figure 5D) in the spleen. The ratio of CD45$^+$ cells had not significantly changed (figure 5E), while an enhanced ratio of CD11c$^+$ DCs (figure 5F) and CD103$^+$ DCs (figure 5G) in CD45$^+$ leucocytes of mEC25 tumours was detected in the mCAF-shWnt2 group compared with that in the control group. Additionally, an enhanced ratio of CD11c$^+$ DCs (figure 5H) or CD103$^+$ DCs (figure 5I) to CD11b$^+$ cells and fewer inhibitory DCs (figure 5J) were induced by interfering with Wnt2 expression in mCAFs. The suppression of DC differentiation by CAF-secreted WNT2 would lead to a reduction in the number of activated DCs, which are responsible for priming CD8$^+$ T cells. A reduction in Wnt2 expression in mCAFs restored the ratio of activated DCs with increased TNFα or IL12 expression and the ratio of mature DCs with CD80 or CD86 expression (figure 5K–N). These in vivo data suggest that CAFs-secreted WNT2 has an important role in suppressing DC-mediated antitumour T-cell responses by inhibiting DC immune-stimulating functions.

WNT2 suppresses the differentiation and immune-stimulating activities of DCs by upregulating SOCS3

We next explored the molecular pathway via which WNT2 regulates DC differentiation and activation. RNA sequencing analysis was performed in DCs subjected to four different treatment methods, including control CM, mWnt2, mCAF.CM and mCAF.CM+αWNT2 treatment. mCAF.CM treatment versus control and mCAF.CM+αWNT2 versus mCAF.CM treatment displayed common changes in 223 (10.6%) genes (online supplemental figure 8A). Gene ontology functional annotation analysis further showed that these common differentially expressed genes were associated with immune signalling pathways, including the TNF, JAK-STAT and NF-κB signalling pathways (online supplemental figure 8B). Of the 223 common genes, suppressor of cytokine signalling 3 (*Socs3*) was identified as one of the most significantly upregulated genes in both mWnt2-treated and mCAF CM-treated DCs (figure 6A). SOCS3 is involved in the regulation of DC differentiation and functions.[27 28] The upregulation of SOCS3 induced by mCAF.CM or mWnt2 in DCs was confirmed by both qPCR (figure 6B) and western blotting (figure 6C). Anti-WNT2 treatment blocked the upregulation of SOCS3 induced by mCAF.CM or mWnt2 in DCs (figure 6B,C). SOCS3 is an endogenous inhibitor of JAK-STAT signalling, which is critical for GM-CSF-mediated CD103$^+$ DC differentiation.[29] Thus, the inhibition of JAK-STAT signalling could be a downstream target of WNT2-induced SOCS3 for the regulation of DC differentiation and function. The phosphorylation of JAK2 and STAT3 (Tyr 705) was inhibited by the mWnt2 protein, while anti-WNT2 treatment abolished this inhibition (figure 6C). Importantly, the reduction in SOCS3 (figure 6D) in DC precursors or DCs improved their differentiation ability (figure 6E,F) and activation (figure 6G), respectively, thereby overcoming WNT2-induced suppression of DC differentiation and activation (figure 6E–G). SOCS3 reduction in DC precursors also attenuated WNT2-induced inhibition of JAK2/STAT3 phosphorylation (figure 6H), suggesting the inhibition of JAK2/STAT3 phosphorylation induced by WNT2 is mediated by the upregulation of SOCS3. Moreover, inhibiting the phosphorylation of STAT3 (Tyr 705) using Napabucasin (2 μM) showed a similar effect on suppressing DC differentiation and function compared with the results using the mWnt2 protein (online supplemental figure 9). Consistent with the in vitro data, in the animal model established by subcutaneous injection of mEC25 cells and mCAFs, a reduced level of SOCS3 (figure 6I) and enhanced STAT3 phosphorylation of CD45$^+$ leucocytes (figure 6J) were detected in tumour tissue of the mCAF-shWnt2 group compared with these values in the control group. Taken together, these findings suggest WNT2 can suppress DC differentiation by upregulating SOCS3 expression and inhibiting JAK2/STAT3 signalling.

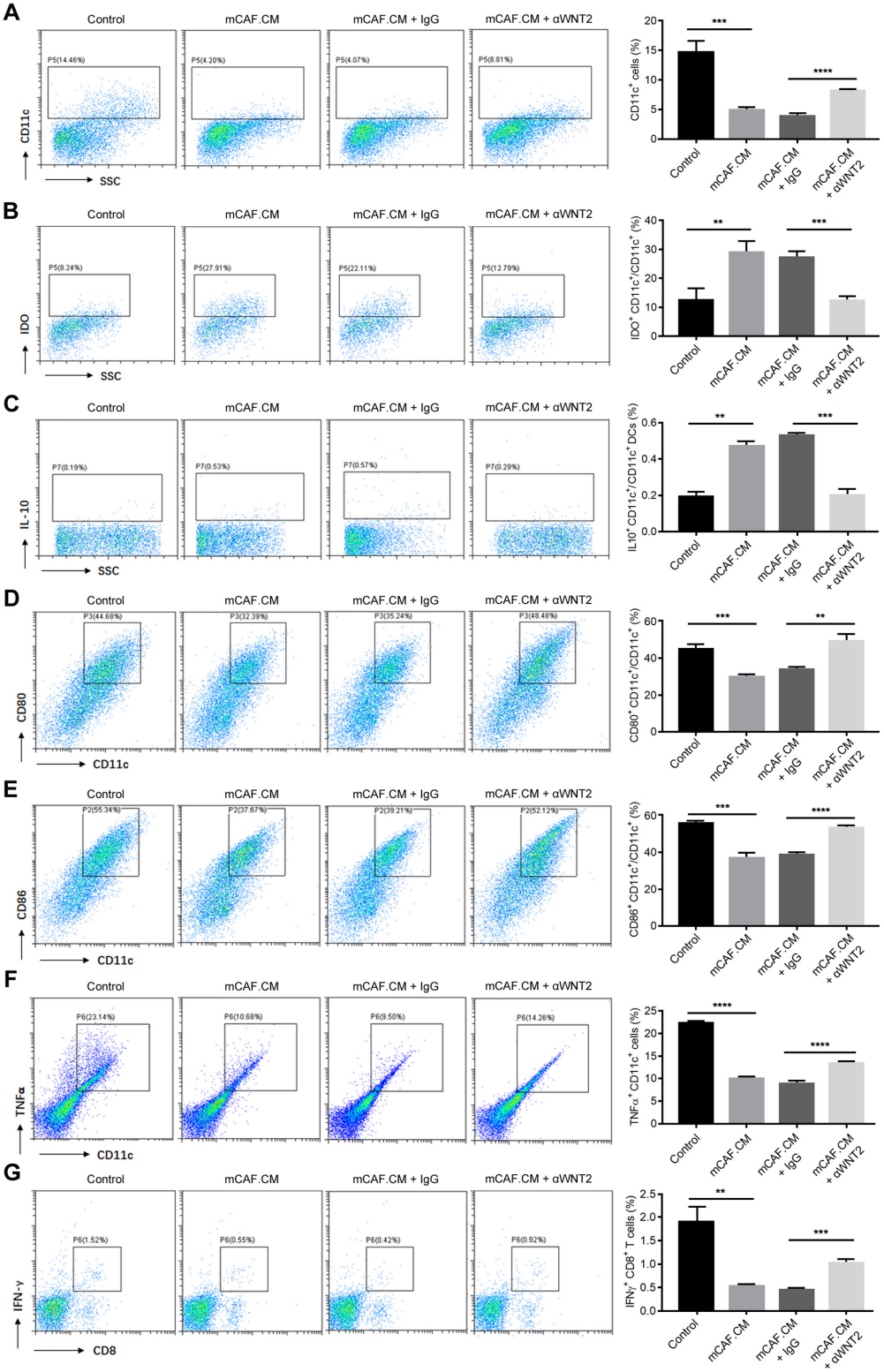

Figure 3 Anti-WNT2 treatment blocked the ability of cancer-associated fibroblasts (CAFs) to suppress dendritic cell (DC) differentiation. (A–C) Flow cytometry was used to quantify the percentage of $CD11c^+$ cells (A), the ratios of inhibitory IDO^+CD11c^+ DCs (B) and $IL10^+CD11c^+$ DCs (C) in mCAF.CM-treated, mCAF.CM+IgG-treated or mCAF.CM+α-WNT2-treated C57BL/6 bone marrow cells when they were induced to DCs with interleukin (IL)-4+granulocyte/macrophage colony-stimulating factor (GM-CSF). Control: RPMI 1640 medium containing 10% FBS with GM-CSF (10 ng/mL)+IL-4 (10 ng/mL); mCAF.CM: culture medium (CM) of CAFs from primary mouse OSCC tumours mixed with control medium (ratio: 1:1). (D–F) Flow cytometry was used to quantify the ratio of $CD80^+CD11c^+$ cells (D), $CD86^+CD11c^+$ cells (E) and the percentage of $TNF\alpha^+CD11c^+$ cells (F) to examine the stimulating activity of DCs. (G) Flow cytometry was used to evaluate the percentage of interferon (IFN)-γ^+ $CD8^+$ T cells after coincubation with mEC25 cell lysate-stimulated DCs for 5 days. For the flow cytometry analyses (A–G), the acquired events were gated based on the strategy shown in online supplemental figure 4. In (B) and (C), $CD11c^+$ cells were further gated based on the SSC-A and CD11c-FITC plots, and analysed for percentage of IDO^+CD11c^+ DCs (B) and $IL10^+CD11c^+$ DCs (C). Data are shown as means±SEM. **p<0.01, ***p<0.001, ****p<0.0001, using the Student's t-test.

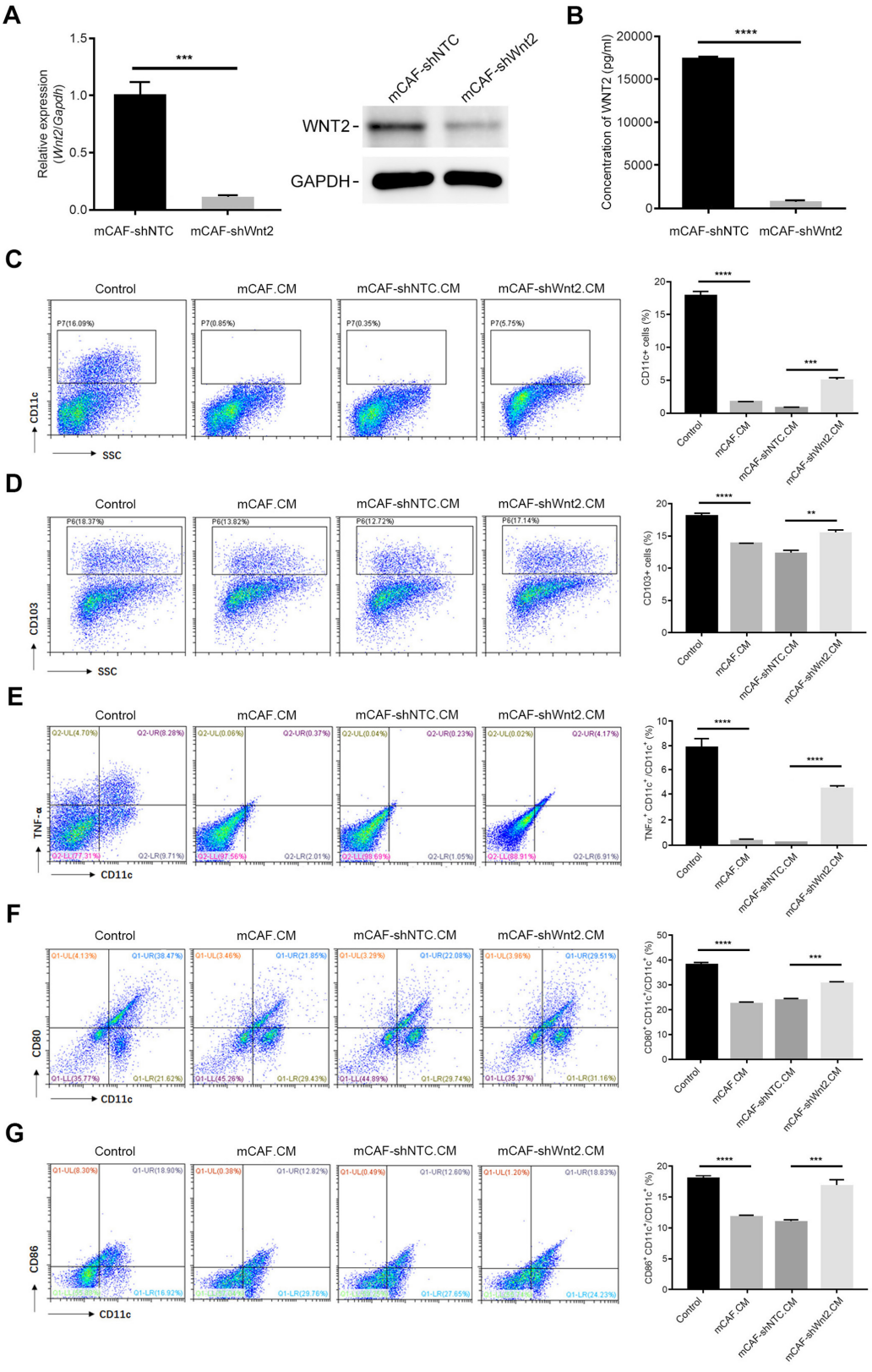

Figure 4 *Wnt2* interference in mCAFs attenuated its inhibition of dendritic cell (DC) differentiation in vitro. (A) Relative expression levels of Wnt2 in mCAF-shNTC or mCAF-shWnt2 were detected using qPCR (left) and western blotting (right). GAPDH was used as an internal control. (B) Wnt2 protein levels in the culture medium of mCAF-shNTC or mCAF-shWnt2 was measured by ELISA. (C and D) Flow cytometry was used to quantify the percentage of $CD11c^+$ cells (C) or $CD103^+$ cells (D) in the mCAF-shNTC.CM-treated or mCAF-shWnt2.CM-treated C57BL/6 bone marrow cells during their induction with interleukin 4+granulocyte/macrophage colony-stimulating factor. (E–G) Flow cytometry was used to quantify the ratios of $TNF\alpha^+CD11c^+$ cells (E), $CD80^+CD11c^+$ cells (F) and $CD86^+CD11c^+$ cells (G) to examine the stimulating activity of DCs. For the flow cytometry analyses (C–G), the acquired events were gated based on the strategy shown in online supplemental figure 4. Data are shown as means±SEM. **p<0.01, ***p<0.001, ****p<0.0001, using the Student's t-test.

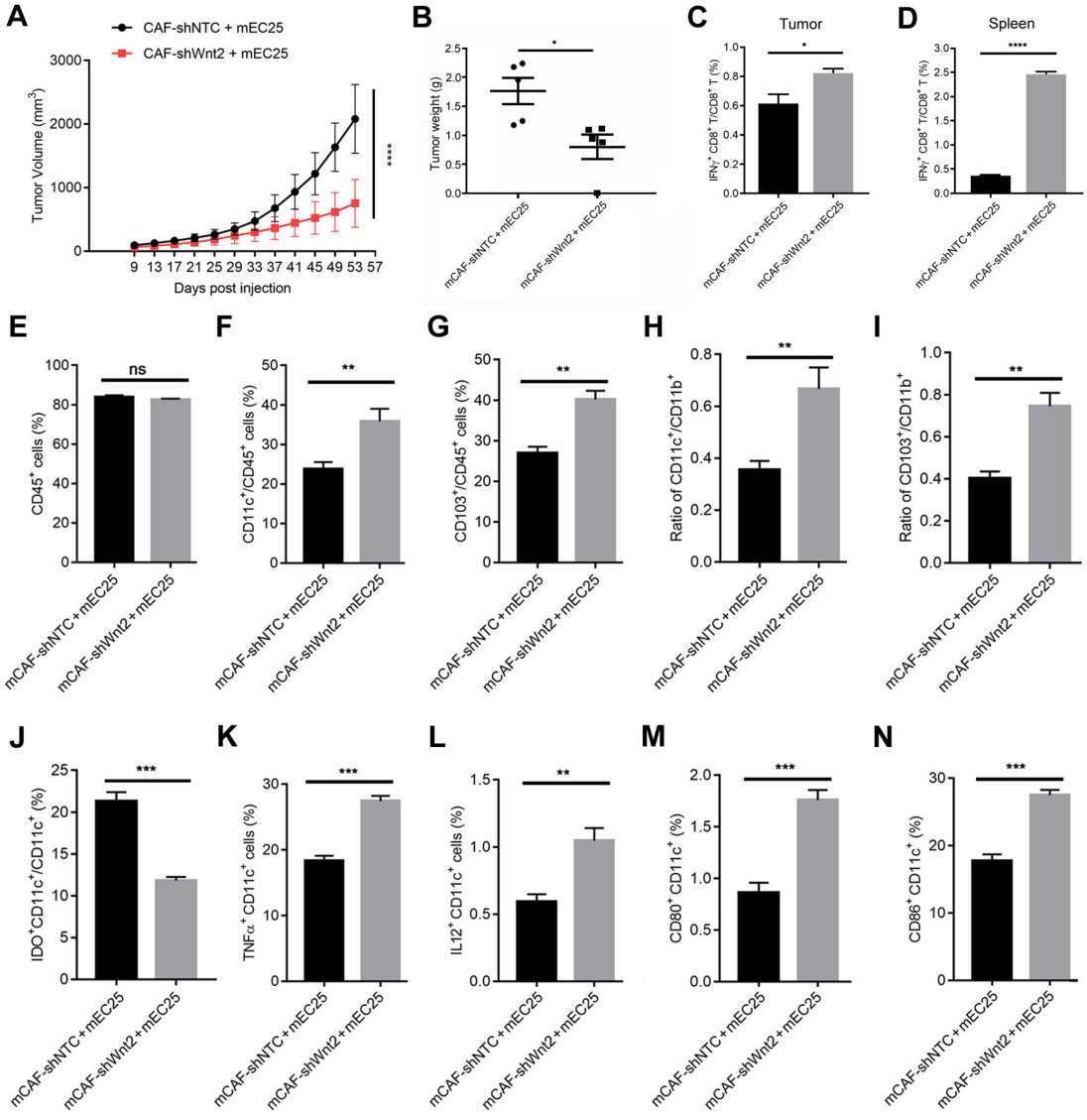

Figure 5 *Wnt2* interference in mCAFs attenuated its in vivo tumour-promoting ability. (A) Average tumour growth curves in mice implanted with mEC25 cells and mCAF-shNTC or mCAF-shWnt2 clones (ratio: 3:1). (B) Tumour weights were presented as means±SEM from five mice per group. (C, D) Flow cytometry was used to quantify the ratio of interferon-γ$^+$CD8$^+$ T cells in lymphocytes isolated from tumour or splenic tissues in (A). (E–G) Flow cytometry was used to evaluate the percentage of CD45$^+$ cells (E) and the ratios of CD11c$^+$CD45$^+$ cells (F) and CD103$^+$CD45$^+$ cells (G) in lymphocytes isolated from mouse tumour tissues in (A). (H–J) Flow cytometry was used to quantify the ratio of CD11c$^+$ dendritic cells (DCs) (H) or CD103$^+$ DCs (I) to CD11b$^+$ cells and inhibitory DCs (J) in tumour tissues. (K–N) Flow cytometry was used to evaluate the percentage of TNFα$^+$ CD11c$^+$ cells (K), IL12$^+$ CD11c$^+$ cells (L), CD80$^+$ CD11c$^+$ cells (M) or CD86$^+$ CD11c$^+$ cells (N) in tumour tissues. Data are shown as means±SEM. *p<0.05, **p<0.01, ***p<0.001, ****p<0.0001 by two-way analysis of variance (ANOVA) in (A) or the Student's t-test in (B–N).

DISCUSSION

Our current study revealed that CAFs-secreted WNT2 has a critical role in regulating tumour immune evasion by suppressing DC differentiation. Anti-WNT2 therapy enhanced the level of antigen-presenting DCs within tumours and thus improved the DC-mediated specific CD8$^+$ T-cell response to tumours, leading to the suppression of tumour progression. Interestingly, anti-WNT2 therapy significantly enhanced the treatment efficacy of anti-PD-1 in syngeneic mouse tumour models. Although anti-PD-1 therapy has shown promising results in the treatment of various cancers, the objective response rate of anti-PD-1 therapy in these cancers remained relatively low.[1 2] The blockade of other signalling pathways that directly suppress the tumour-killing functions of effective CD8$^+$ T cells, such as inhibition of the CTLA-4 pathway, has been used to improve the results of treatments that use immune checkpoint inhibition.[9] However, the low level of effective CD8$^+$ T cells in tumours negatively affects the efficacy of these therapies.[30] Effective synergy for killing tumour cells could be gained by enhancing the level of intratumoural effective CD8$^+$ T cells and blocking immune checkpoints that negatively regulate the activation of effector T cells. In addition to enhancing the infiltration of CD8$^+$ T cells into tumours, promoting the generation of effective cytotoxic T lymphocytes could be an alternative way to increase intratumoural effective CD8$^+$ T cells. Based on our findings, combined therapy using both anti-WNT2 and anti-PD-1 antibodies has the advantage of simultaneously rescuing the initiation of tumour-specific effective CD8$^+$ T cells and activating these

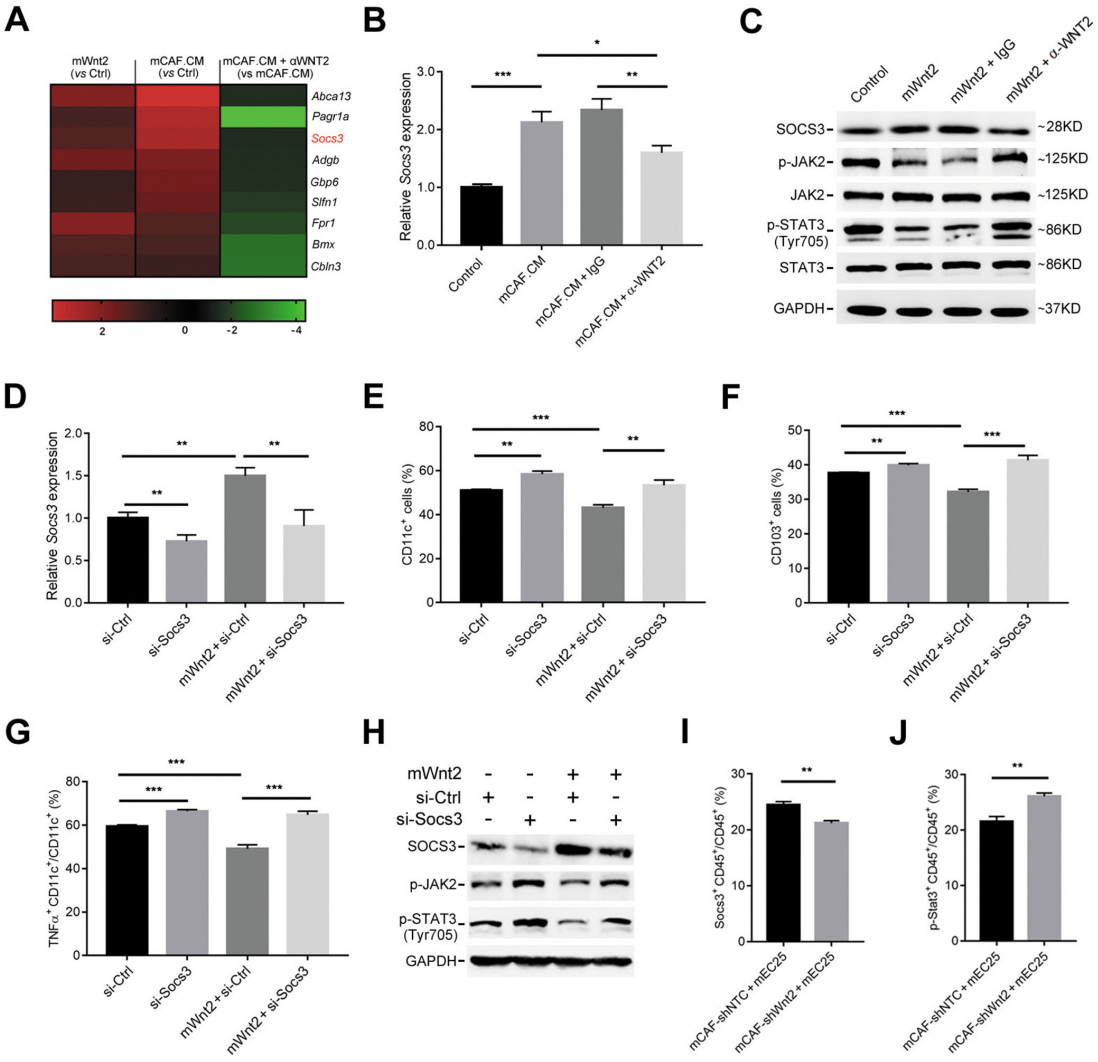

Figure 6 WNT2 regulates dendritic cell (DC) differentiation by upregulating SOCS3 expression. (A) A heatmap of nine genes which were commonly upregulated in mWnt2-treated and mCAF.CM-treated DCs compared with their expression in control culture medium (CM)-treated DCs, and downregulated in mCAF.CM+αWNT2-treated DCs compared with their expression in mCAF.CM-treated DCs. (B) The relative expression levels of SOCS3 in control CM-treated, mCAF.CM-treated, mCAF.CM+IgG-treated and mCAF.CM+αWNT2-treated DCs were detected by qPCR. (C) SOCS3 protein expression and the activation of JAK2/STAT3 signalling in control CM-treated, mWnt2-treated, mWnt2+IgG-treated and mWnt2+αWNT2-treated DCs were assessed by western blotting. (D) The relative expression level of SOCS3 was detected by qPCR with or without mWnt2 (100 ng/mL) treatment in si-SOCS3 or si-Control (Ctrl) transfected DC precursors during DC induction. (E–G) Flow cytometry was used to evaluate the percentage of $CD11c^+$ cells (E) or $CD103^+$ cells (F) and the ratio of $TNF\alpha^+CD11c^+$ cells (G) in DCs treated as described in (D). (H) Western blotting showed JAK2/STAT3 activation in DC precursors treated as described in (D). (I, J) Flow cytometry was used to evaluate the ratios of $SOCS3^+CD45^+$ cells (I) and $p\text{-}STAT3^+CD45^+$ cells (J) in lymphocytes isolated from mouse tumour tissues as described in figure 5. Data are shown as means±SEM. *p<0.05, **p<0.01, ***p<0.001, using the Student's t-test.

effector T cells, both of which are inhibited by TME-derived factors (figure 7).

WNT2 is highly expressed in various cancers, including oesophageal cancer,[11] colon cancer[13] and GC.[14 17] Therefore, anti-WNT2 therapy could be used alone or in combination with other immunotherapeutic approaches to treat these GI cancers, by enhancing the antitumour immune response. It is worth noting that WNT2 is generally absent in healthy human tissues, except the placenta[31] and endometrium.[32] No obvious toxicity was induced in mice by anti-WNT2 treatment in our study, suggesting WNT2-targeted therapy would be safe for cancer treatment. Pan-inhibitors of the Wnt/β-catenin pathway have been used to treat different cancers in several clinical trials.[33 34] However, some members of the WNT family and their downstream effectors are essential for the normal functioning of vital organs, and may not therefore represent a good therapeutic target for cancer treatment. For example, WNT5A is highly expressed in the lungs and plays an important role in regulating their biological function.[35 36] Therefore, a specific anti-WNT2 antibody may be safer and more effective than pan-inhibitors of the Wnt/β-catenin pathway in the treatment of GI tumours with WNT2 overexpression.

Due to the lack of mouse OSCC cell line, studies for CAFs-regulated antitumour immunity in OSCC is scanty. Taking advantage of a mouse OSCC cell line mEC25 generated in our group, we are able to reveal a novel mechanism in which CAFs regulate the antitumour immunity in OSCC. CAFs from oesophageal and colon cancers can use their secreted WNT2 to suppress antitumour immune responses. Depletion of WNT2-secreting CAFs would therefore improve the antitumour immune response in the TME and suppress tumour progression. It has been suggested that

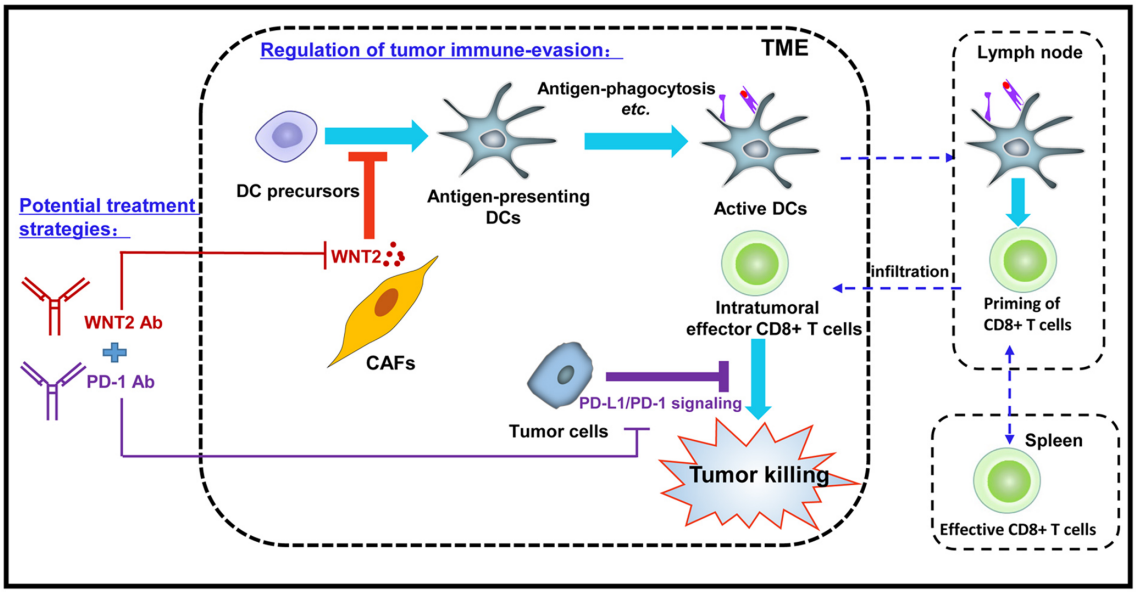

Figure 7 Proposed mechanism of cancer-associated fibroblasts (CAFs)-derived WNT2 in regulating antitumour immunity. CAFs secreted WNT2 inhibited the dendriticcell (DC) differentiation and DC-mediated antitumour T-cell responses in tumour microenvironment (TME). Anti-WNT2 therapy significantly restored antitumour T-cell responses within tumours and enhanced the efficacy of anti-programmed cell death protein 1 (PD-1) by increasing active DC.

CAF depletion may attenuate the generation of matrix and impair the tumour barrier, thus enhancing the infiltration of antitumour drugs.[37] Therefore, employing a strategy of depleting WNT2-secreting CAFs in combination with PD-1 antibodies could not only work to improve antitumour immune responses but also enhance the infiltration of PD-1 antibodies into tumours. In oesophageal cancer, WNT2 is mainly secreted by FGFR2$^+$ CAFs.[10] However, FGFR2 is also highly expressed in healthy tissues, including the brain,[38] skin[39] and bone marrow.[40] Therefore, the identification of more specific surface markers of WNT2-secreting CAFs will be required to develop novel CAF-depletion strategies that can be used to improve the efficiency of anti-PD-1 therapy in OC (oesophageal cancer) and CRC.

DC differentiation is suppressed by tumour-derived or TME-derived factors, such as fibrinogen-like protein 2, which is highly expressed in glioma stem cells, and this suppression of DC differentiation plays a critical role in promoting tumour progression.[29] Our data suggested CAF-derived WNT2 inhibited the differentiation of CD11c$^+$ DCs and CD103$^+$ DCs in tumours and thus attenuated the level of tumour-antigen presentation and CD8$^+$ T-cell priming, without affecting the intratumoural infiltration of CD45$^+$ cells. The activation of JAK2/STAT signalling is important for maintaining the differentiation of CD103$^+$ DCs.[29] Our results confirmed that the p-JAK2/p-STAT3 (Tyr705) pathway plays an essential role in maintaining the differentiation of DCs. WNT2 inhibited the activation of JAK2/STAT3 through the upregulation of SOCS3 in DC precursors. Previous studies have shown that SOCS3 is critical for regulating the function of immune cells,[27 28] but it remains unclear whether SOCS3 is involved in the regulation of tumour immune-evasion. In the present study, we provide the first evidence that the expression of SOCS3 in DC precursors mediates the regulation of DC differentiation in tumours, indicating it may serve as a novel target for cancer therapy. In the future, however, it will be critical to develop an appropriate therapeutic strategy by targeting DC-derived SOCS3. Different studies have produced contradictory results with regard to the role played by JAK2/STAT signalling in the regulation of immune-cell functions. While some studies have shown that activation of the JAK2/STAT pathway is required for the differentiation of DCs and thus the maintenance of the DC-mediated T-cell response,[29 41] others have shown that tumour-derived factors can impair the antitumour activities of DCs by activating JAK2/STAT signalling.[42 43] This inconsistency might reflect the different roles played by JAK2/STAT signalling in regulating antitumour immune responses within different TMEs.

Taken together, our findings revealed a novel mechanism in which CAFs-secreted WNT2 regulates immune-evasion processes of tumour cells and showed that anti-WNT2 therapy could effectively improve the treatment efficacy of anti-PD-1. These findings may open a new window on our understanding of the role played by CAFs in regulating antitumour immunity and provide new directions for developing more efficient immunotherapy strategies for GI cancers.

Correction notice This article has been corrected since it published Online First. The first author statement has been added.

Contributors T-XH, X-YT and H-SH acquired the animal data. T-XH, X-YT, H-SH and Y-TL performed the in vitro cell experiments. B-LL, ZC and XYG acquired the patient-tissue IHC data. K-SL, XC and CZ acquired the antibody binding data. T-XH and LF designed the study, analysed the data and wrote the manuscript. LF supervised the study and revised the manuscript.

Funding This work was supported by grants from the National Key R&D Programme of China (2017YFA0503900), the National Natural Science Foundation of China (81372583 and 81772957), the Science and Technology Programme of Guangdong Province in China (2019B030301009), the Industry and Information Technology Foundation of Shenzhen (20180309100135860), the Shenzhen Basic Research Programme (JCYJ20200109113810154), the SZU Top Ranking Project (86000000210) and the RGC CRF Project (C7065-18GF).

Competing interests None declared.

Patient consent for publication Not required.

Provenance and peer review Not commissioned; externally peer reviewed.

Data availability statement Data are available in a public, open access repository. All data relevant to the study are included in the article or uploaded as

supplementary information. Data are available in public, open access repositories, directly included in the article, uploaded as supplementary information from first or last authors. RNA-seq data are publicly available through the NIH GEO platform (https://www.ncbi.nlm.nih.gov/geo/): GEO accession no. GSE154420.

ORCID iD

Li Fu http://orcid.org/0000-0003-2643-6278

REFERENCES

1 Tang J, Yu JX, Hubbard-Lucey VM, *et al*. Trial watch: the clinical trial landscape for PD1/PDL1 immune checkpoint inhibitors. *Nat Rev Drug Discov* 2018;17:854–5.
2 Zhao P, Li L, Jiang X, *et al*. Mismatch repair deficiency/microsatellite instability-high as a predictor for anti-PD-1/PD-L1 immunotherapy efficacy. *J Hematol Oncol* 2019;12:54.
3 Chen L, Han X. Anti-PD-1/PD-L1 therapy of human cancer: past, present, and future. *J Clin Invest* 2015;125:3384–91.
4 Baumeister SH, Freeman GJ, Dranoff G, *et al*. Coinhibitory pathways in immunotherapy for cancer. *Annu Rev Immunol* 2016;34:539–73.
5 Rabinovich GA, Gabrilovich D, Sotomayor EM. Immunosuppressive strategies that are mediated by tumor cells. *Annu Rev Immunol* 2007;25:267–96.
6 Orimo A, Gupta PB, Sgroi DC, *et al*. Stromal fibroblasts present in invasive human breast carcinomas promote tumor growth and angiogenesis through elevated SDF-1/CXCL12 secretion. *Cell* 2005;121:335–48.
7 Kraman M, Bambrough PJ, Arnold JN, *et al*. Suppression of antitumor immunity by stromal cells expressing fibroblast activation protein-alpha. *Science* 2010;330:827–30.
8 Wen Y, Wang C-T, Ma T-T, *et al*. Immunotherapy targeting fibroblast activation protein inhibits tumor growth and increases survival in a murine colon cancer model. *Cancer Sci* 2010;101:2325–32.
9 Huang T-X, Fu L. The immune landscape of esophageal cancer. *Cancer Commun* 2019;39:79.
10 Zhang C, Fu L, Fu J, *et al*. Fibroblast growth factor receptor 2-positive fibroblasts provide a suitable microenvironment for tumor development and progression in esophageal carcinoma. *Clin Cancer Res* 2009;15:4017–27.
11 Fu L, Zhang C, Zhang L-Y, *et al*. Wnt2 secreted by tumour fibroblasts promotes tumour progression in oesophageal cancer by activation of the Wnt/β-catenin signalling pathway. *Gut* 2011;60:1635–43.
12 Logan CY, Nusse R. The Wnt signaling pathway in development and disease. *Annu Rev Cell Dev Biol* 2004;20:781–810.
13 Kramer N, Schmöllerl J, Unger C, *et al*. Autocrine WNT2 signaling in fibroblasts promotes colorectal cancer progression. *Oncogene* 2017;36:5460–72.
14 Zhang Z, Wang J, Dong X. Wnt2 contributes to the progression of gastric cancer by promoting cell migration and invasion. *Oncol Lett* 2018;16:2857–64.
15 Xiu D-H, Liu G-F, Yu S-N, *et al*. Long non-coding RNA LINC00968 attenuates drug resistance of breast cancer cells through inhibiting the Wnt2/β-catenin signaling pathway by regulating WNT2. *J Exp Clin Cancer Res* 2019;38:94.
16 Dale TC, Weber-Hall SJ, Smith K, *et al*. Compartment switching of WNT-2 expression in human breast tumors. *Cancer Res* 1996;56:4320–3.
17 Katoh M. WNT2 and human gastrointestinal cancer (review). *Int J Mol Med* 2003;12:811–6.
18 Staal FJT, Luis TC, Tiemessen MM. WNT signalling in the immune system: WNT is spreading its wings. *Nat Rev Immunol* 2008;8:581–93.
19 Xiao J, Zhou H, Wu N, *et al*. The non-canonical Wnt pathway negatively regulates dendritic cell differentiation by inhibiting the expansion of Flt3(+) lymphocyte-primed multipotent precursors. *Cell Mol Immunol* 2016;13:593–604.
20 Zhou J, Cheng P, Youn J-I, *et al*. Notch and wingless signaling cooperate in regulation of dendritic cell differentiation. *Immunity* 2009;30:845–59.
21 Wang B, Tian T, Kalland K-H, *et al*. Targeting Wnt/β-catenin signaling for cancer immunotherapy. *Trends Pharmacol Sci* 2018;39:648–58.
22 Spranger S, Bao R, Gajewski TF. Melanoma-intrinsic β-catenin signalling prevents anti-tumour immunity. *Nature* 2015;523:231–5.
23 Zhao F, Xiao C, Evans KS, *et al*. Paracrine Wnt5a-β-Catenin signaling triggers a metabolic program that drives dendritic cell Tolerization. *Immunity* 2018;48:147–60.
24 Huang T, Perez-Cordon G, Shi L, *et al*. Clostridium difficile toxin B intoxicated mouse colonic epithelial CT26 cells stimulate the activation of dendritic cells. *Pathog Dis* 2015;73:ftv008.
25 Gardner A, Ruffell B. Dendritic cells and cancer immunity. *Trends Immunol* 2016;37:855–65.
26 Huang T, Yang J, Liu B, *et al*. A new mouse esophageal cancer cell line (mEC25)-derived pre-clinical syngeneic tumor model for immunotherapy. *Cancer Commun* 2020;40:316–20.
27 Li Y, Chu N, Rostami A, *et al*. Dendritic cells transduced with SOCS-3 exhibit a tolerogenic/DC2 phenotype that directs type 2 th cell differentiation in vitro and in vivo. *J Immunol* 2006;177:1679–88.
28 Li Y, de Haar C, Peppelenbosch MP, *et al*. SOCS3 in immune regulation of inflammatory bowel disease and inflammatory bowel disease-related cancer. *Cytokine Growth Factor Rev* 2012;23:127–38.
29 Yan J, Zhao Q, Gabrusiewicz K, *et al*. FGL2 promotes tumor progression in the CNS by suppressing $CD103^+$ dendritic cell differentiation. *Nat Commun* 2019;10:448.
30 Teng MWL, Ngiow SF, Ribas A, *et al*. Classifying cancers based on T-cell infiltration and PD-L1. *Cancer Res* 2015;75:2139–45.
31 Ferreira JC, Choufani S, Grafodatskaya D, *et al*. WNT2 promoter methylation in human placenta is associated with low birthweight percentile in the neonate. *Epigenetics* 2011;6:440–9.
32 Bui TD, Zhang L, Rees MC, *et al*. Expression and hormone regulation of WNT2, 3, 4, 5a, 7a, 7b and 10b in normal human endometrium and endometrial carcinoma. *Br J Cancer* 1997;75:1131–6.
33 Krishnamurthy A, Dasari A, Noonan AM, *et al*. Phase Ib results of the rational combination of selumetinib and cyclosporin A in advanced solid tumors with an expansion cohort in metastatic colorectal cancer. *Cancer Res* 2018;78:5398–407.
34 Ahmed K, Shaw HV, Koval A, *et al*. A second Wnt for old drugs: drug repositioning against WNT-Dependent cancers. *Cancers* 2016;8:66.
35 Li C, Hu L, Xiao J, *et al*. Wnt5a regulates Shh and Fgf10 signaling during lung development. *Dev Biol* 2005;287:86–97.
36 Li C, Xiao J, Hormi K, *et al*. Wnt5a participates in distal lung morphogenesis. *Dev Biol* 2002;248:68–81.
37 Loeffler M, Krüger JA, Niethammer AG, *et al*. Targeting tumor-associated fibroblasts improves cancer chemotherapy by increasing intratumoral drug uptake. *J Clin Invest* 2006;116:1955–62.
38 Frinchi M, Bonomo A, Trovato-Salinaro A, *et al*. Fibroblast growth factor-2 and its receptor expression in proliferating precursor cells of the subventricular zone in the adult rat brain. *Neurosci Lett* 2008;447:20–5.
39 Czyz M. Fibroblast growth factor receptor signaling in skin cancers. *Cells* 2019;8:540.
40 Shigematsu A, Shi M, Okigaki M, *et al*. Signaling from fibroblast growth factor receptor 2 in immature hematopoietic cells facilitates donor hematopoiesis after intra-bone marrow-bone marrow transplantation. *Stem Cells Dev* 2010;19:1679–86.
41 Zhong J, Yang P, Muta K, *et al*. Loss of Jak2 selectively suppresses DC-mediated innate immune response and protects mice from lethal dose of LPS-induced septic shock. *PLoS One* 2010;5:e9593.
42 Melillo JA, Song L, Bhagat G, *et al*. Dendritic cell (DC)-specific targeting reveals Stat3 as a negative regulator of DC function. *J Immunol* 2010;184:2638–45.
43 Alshamsan A, Hamdy S, Das S, *et al*. Validation of bone marrow derived dendritic cells as an appropriate model to study tumor-mediated suppression of DC maturation through STAT3 hyperactivation. *J Pharm Pharm Sci* 2010;13:21–6.

Targeting cancer-associated fibroblast-secreted WNT2 restores dendritic cell-mediated anti-tumor immunity

Tu-Xiong Huang,[1,2] Xiang-Yu Tan,[1] Hui-Si Huang,[1] Yu-Ting Li,[1] Bei-Lei Liu,[3] Kai-Sheng Liu,[2] Xin-Chun Chen,[1] Zhe Chen,[4] Xin-Yuan Guan,[3] Chang Zou,[2] Li Fu[1*]

[1]Guangdong Provincial Key Laboratory of Regional Immunity and Diseases, Department of Pharmacology and Shenzhen University International Cancer Center, Shenzhen University Health Science Center, Shenzhen 518060, Guangdong, P. R. China;

[2]Shenzhen People's Hospital (The Second Clinical Medical College, Jinan University; The First Affiliated Hospital, Southern University of Science and Technology), Shenzhen 518020, Guangdong, China;

[3]Department of Clinical Oncology, The University of Hong Kong, Hong Kong;

[4]Key Laboratory of Digestive Pathophysiology of Zhejiang Province, First Affiliated Hospital, Zhejiang Chinese Medical University, Hangzhou, 310053, China.

*Correspondence to

Dr Li Fu, Department of Pharmacology and Shenzhen University International Cancer Center, Shenzhen University Health Science Center, Shenzhen 518060, China; gracelfu@szu.edu.cn

Huang T, *et al. Gut* 2021;0:1–12. doi: 10.1136/gutjnl-2020-322924

SUPPLEMENTAL MATERIALS AND METHODS

Double immunofluorescence (IF)

The FFPE archived ESCC tissue sections were deparaffinized and treated with 10 mM citrate buffer (pH 6.0) at 95–100 °C for 15 min. After washing three times with phosphate-buffered saline (PBS; Gibco), the slides were treated with 0.25% Triton X-100 for 10 min and then blocked in 10% bovine serum albumin (BSA) in PBS for 1 h. A mixture of two primary antibodies (rabbit against WNT2 and mouse against FGFR2; rabbit against CD4 and mouse against FOXP3; rabbit against CD8 and mouse against IFN-γ; Abcam) was incubated overnight at 4 °C. Following washing, the slides were incubated for 1 h at room temperature with a mixture of two secondary antibodies (Alexa Fluor594-conjugated anti-rabbit IgG and Alexa Fluor488-conjugated anti-mouse IgG, or Alexa Fluor488-conjugated anti-rabbit IgG and Alexa Fluor594-conjugated anti-mouse IgG; Invitrogen) and Hoechst 33342 (Invitrogen) counterstain. Slides were subsequently mounted with ProLong™ Diamond Antifade Mountant (Invitrogen). Images were acquired using the Tissue FAXS Systems (TissueGnostics) and analyzed with TissueFAXS Imaging Software.

Clinical samples and cell lines

A total of 47 formalin-fixed and paraffin-embedded (FFPE) ESCC tissues were collected from the Shenzhen People's Hospital. All clinical samples used in this study were approved by the Committee for Ethical Review of Research at Shenzhen People's Hospital. The mouse ESCC cell line, mEC25, was established in our laboratory.[1] CMT93 mouse CRC cell line and 293T cell line were obtained from

the American Type Culture Collection. All cell lines were cultured in high-glucose DMEM (Gibco) supplemented with 10% fetal bovine serum (FBS; Gibco) and incubated at 37 °C in a humidified chamber containing 5% CO_2.

Generation of anti-WNT2 and anti-WNT2 Fab antibodies

The mouse monoclonal anti-WNT2 (3C4), which was custom-made at Kexing Biotech Inc (Hangzhou, China), is a IgG1 type antibody against human and mouse WNT2 protein. Anti-WNT2 Fab was generated based on anti-WNT2 IgG (3C4) by removing Fc fragment with enzymatic digestion methods.

Isolation of primary mouse CAFs (mCAFs)

mCAFs were isolated from mouse primary ESCC tumors that had been induced by the carcinogen 4-nitroquinoline-1-oxide (4-NQO), as previously described.[1 2] Briefly, freshly collected mouse ESCC tumor tissue was cut into pieces that were as small as possible in sterile PBS solution, followed by digestion with collagenase IV (1 mg/ml; Sigma). The suspension was filtered through the membrane of a 70-μm cell-strainer to collect a suspension of single cells. The filtrate was centrifuged, washed twice, then plated on 60-mm tissue culture dishes in 5 ml DMEM medium containing 10% FBS. After culturing for 45 min at 37 °C, non-adherent cells (mainly tumor cells) were removed to obtain pure fibroblasts. Non-tumorous esophageal tissues were used to isolate normal fibroblasts (NFs), as described above.

Lentivirus vector preparation and primary cell transduction

Lentivirus was generated with a packaging mix (Sigma) and pLKO.1-Puro-shWnt2 plasmid (Sigma) or pLKO.1-Puro-shNTC control plasmid (Sigma), according to the manufacturer's protocol. Primary mCAFs were transduced by shWnt2 of shNTC lentivirus. Puromycin (Sigma) was used to select mCAF-shWnt2 or mCAF-shNTC stable clones. The sequences for the *Socs3*-targeted siRNA and control siRNA were designed and synthesized by GenePharma (Suzhou, China); these sequences are shown in online supplementary table 1. siRNAs were transfected into primary DC precursors with Lipofectamine 3000 (Invitrogen).

Cytotoxic T lymphocyte (CTL) assay

$CD8^+$ T cells were isolated from spleens of C57BL/6 mice, using a negative $CD8^+$ T-cell isolation kit (Stemcell Technologies) and following the manufacturer's instructions. These effector $CD8^+$ T cells were re-stimulated with tumor lysate for 3 days and were then tested for cytolytic activity against mEC25 cells or CMT93 cells (effector cells : target cells = 50 : 1) using a cytotoxicity detection kit (LDH) (Roche Applied Science, Indianapolis, IN, USA), according to the manufacturer's instructions.

RNA extraction and quantitative real-time PCR

Total RNA from mCAFs or DC precursors was extracted using TRIzol Reagent (Invitrogen) and reversed-transcribed with PrimeScript™ RT-PCR Kit (Takara). Real-time PCR for analyzing Wnt2 or SOCS3 mRNA levels was performed with TB Green® Premix Ex Taq™ (Takara), according to the manufacturer's instructions, on a CFX Connect Real-Time PCR Detection System (Bio-Rad). Data

were normalized by the level of GAPDH mRNA in each individual sample. The $2^{-\Delta\Delta Ct}$ method was used to calculate relative changes in expression.

Western blotting

Western blotting was performed according to the standard protocol, using antibodies for SOCS3 (Abcam), JAK2 (D2E12; CST), p-JAK2 (D15E2; CST), STAT3 (79D7; CST), p-STAT3 Tyr705 (D3A7; CST), or GAPDH (D16H11; CST), and then with HRP-conjugated secondary antibody after washing. The bands on the membranes were detected using a Pierce™ Fast Western Blot Kit (Thermo Scientific) and the ChemiDoc Touch Gel Imaging system (Bio-Rad).

RNA sequence analysis

Total RNA from control CM, mWnt2, mCAF.CM, or mCAF.CM+αWNT2 treated DCs was depleted of genomic DNA and rRNA. After purification of the remaining RNA without rRNA, the RNA was fragmented into small pieces using divalent cations under elevated temperature. The cleaved RNA fragments were copied into first strand cDNA using reverse transcriptase and random primers, followed by second strand cDNA synthesis. These cDNA fragments then were subjected to end-repair, phosphorylation and 'A' base addition according to Illumina library construction protocol. Deep sequencing was performed on an Illumina NovaSeq 6000 at WuXi NextCODE (Shanghai, China). RSEM (1.2.29) were used to perform expression abundance quantification based on the uniquely mapped reads. Transcripts with fold change ≥ 2 in expression level were defined as differentially

expressed. Hypergeometric test implemented in GOSTATs was used to perform functional enrichment analysis and gene set enrichment analysis. The RNA-sequencing data generated in this investigation were deposited in the National Center for Biotechnology Information's Gene Expression Omnibus (GEO) database and can be accessed using GEO accession no. GSE154420.

ELISA analysis

Cell culture supernatants of mCAF-shWnt2 or mCAF-shNTC clones were collected, and the concentration of Wnt2 was measured using the mouse Wnt2 ELISA kit (CUSABIO), according to the manufacturer's instructions. For detecting the secretion of TNFα and IL12 by DCs as well as the secretion of IFNγ by $CD8^+$ T cells, the cells were treated as in FACS assay followed by the collection of their culture-supernatant. The concentration of TNFα, IL12, or IFNγ in the culture-supernatant was detected using the corresponding ELISA kit (Biolegend).

Immunohistochemical (IHC) and hematoxylin/eosin (HE) analysis

Isotype IgG or biotin-labeled anti-WNT2 was injected into mEC25-tumor bearing C57BL/6 mice intraperitoneally every two days for three times, and the tumors and normal organs including heart, liver, spleen, lung, and kidney were isolated. Consecutive frozen sections and streptavidin-biotin-HRP complex method were used for IHC analysis. In brief, frozen tissue sections were blocked with 0.3% hydrogen peroxide for 15min, and with 10% normal rabbit serum for 10min, followed by the incubation of streptavidin-biotin-HRP complex. Streptavidin was omitted as the negative staining control. The

slides were visualized using 3, 3'-diaminobenzidine (Dako), and then counterstained with hematoxylin (Sigma-Aldrich). For the histological analyses, consecutive human ESCC tissue sections used for the IF analyses of WNT2$^+$ CAFs, Tregs, and effector CD8$^+$ T cells, or the frozen sections of normal organs from the mice in IgG and anti-WNT2 treatment group, were stained with HE according to the manufacturer's instructions (Vector, Burlingame, CA). The images were captured with Slide Scan System (SQS1000; TEKSQRAY).

Statistical analysis

All quantitative data are presented as means ± standard error of the mean (s.e.m.), unless otherwise indicated. The statistical analyses were performed using an unpaired two-tailed Student's *t*-test or two-way ANOVA, using the Prism statistical software program (GraphPad Software, Inc., San Diego, CA, USA). A P-value less than 0.05 was considered to be significant. *P<0.05, **P<0.01, ***P<0.001,****P<0.0001.

SUPPLEMENTAL FIGURE LEGENDS

Supplementary figure 1 Identification of the specificity and species reactivity of the anti-WNT2 monoclonal antibody. (A) Western blotting revealed that anti-WNT2 monoclonal antibody (Clone: 3C4) specifically recognized the cell lysate of 293T cells with overexpression of human WNT2, but not those with overexpression of human WNT2B, WNT3A, WNT5A, WNT5B, WNT7B, or WNT11. GAPDH was used as an internal control. (B) Western blotting revealed that anti-WNT2 recognized the

cell lysate of 293T cells with mouse Wnt2 overexpression. GAPDH was used as an internal control.

Supplementary figure 2 Anti-WNT2 therapy induced tumor-killing immunity and enhanced the therapeutic efficacy of anti-PD-1 in mouse CRC. (A) Schematic of the drug intervention protocol for α-WNT2 (intraperitoneally) and/or α-PD1 (intraperitoneally) in C57BL/6 mice subcutaneously implanted with CMT93 cells. At the drug intervention end-point, mouse tissues were obtained for flow cytometry. (B) Average tumor growth curves of syngeneic CMT93 tumors in mice treated as described in (A). (C) The visual maps of CMT93 tumors by indicated treatment. The tumors were removed from mice at day 30 after CMT93 cell injection. (D) Flow cytometry was used to quantify the percentage of effective $CD8^+$ T cells ($IFN\gamma^+$) in anti-WNT2, anti-PD-1, and IgG isotype-treated mice (n=5/group). (E) A cytotoxic lymphocyte (CTL) assay evaluated the tumor-killing activity of $CD8^+$ T cells isolated from mice spleen treated in (D). (F-I) Flow cytometry analysis was used to quantify the percentage of $CD11c^+$ DC cells (F), $CD103^+$ DC cells (G), $CD80^+CD11c^+$ DC cells (H), and $CD86^+CD11c^+$ cells (I) in tumors from mice treated in (D). Data are shown as means ± s.e.m. *p<0.05, **p<0.01, ***p<0.001, ****p<0.0001 by two-way ANOVA in (B) or Student's t-test in (D-I).

Supplementary figure 3 Evaluation of the potential off target effects of anti-WNT2. (A,B) IHC analysis was used to evaluate the binding activities of biotin-labeled anti-WNT2 to tumor tissues (A) and normal vital organs including heart, liver, spleen, lung and kidney (B) after intraperitoneal injection into mice. Scale bar: 100μm (Upper panel); 50μm (Lower panel). (C) Representative H&E staining of

normal vital organs from the anti-WNT2-treated and IgG-treated mice. Scale bar: 20μm.

Supplementary figure 4 Gating strategy used for flow cytometry analyses. For the analyses of flow cytometry experiments, the acquired events were firstly gated based on the forward scatter (FSC-A) and side scatter (SSC-A) plots. Single cells were then gated based on the height and area of FSC (FSC-H vs. FSC-A) and analyzed for the indicated cell surface markers which were stained with specific fluorescence-labeled antibodies. The obtained data were processed using Beckman CytExpert software.

Supplementary figure 5 Recombinant mouse-Wnt2 protein inhibited DC differentiation in vitro. (A,B) Flow cytometry was used to evaluate the percentage of $CD11c^+$ cells (A) and $CD103^+$ cells (B) in C57BL/6 bone marrow cells during DC induction with mWnt2 (100 ng/ml), mWnt2+IgG, mWnt2+αWNT2 IgG or mWnt2+αWNT2 Fab treatment. Control: RPMI 1640 medium containing 10% FBS with GM-CSF (10 ng/ml) + IL-4 (10 ng/ml). (C-F) After DC induction with the indicated treatment, the cells were stimulated with LPS, and the percentage of $TNF\alpha^+CD11c^+$ cells (C), $IL12^+CD11c^+$ cells (D), $CD80^+CD11c^+$ cells (E) and $CD86^+CD11c^+$ cells (F) was assessed by flow cytometry. (G) After DC induction with the indicated treatment, the cells were stimulated with mEC25 cell lysate followed by co-incubation with $CD8^+$ T cells for 5 days, and the percentage of $IFN\gamma^+CD8^+$ T cells in $CD8^+$ gated cells was evaluated by flow cytometry. (H-J) ELISA assay was used to detect the secretion of TNFα (H) and IL12 (I) by DCs, and the secretion of IFNγ (J) by $CD8^+$ T cells with the

indicated treatment. For the flow cytometry analyses (A-G), the acquired events were gated based on the strategy shown in online supplementary figure 4. Data are shown as means ± s.e.m. **p<0.01, ***p<0.001, ****p<0.0001, using the Student's t-test. LPS, lipopolysaccharide.

Supplementary figure 6 Recombinant human-WNT2 protein treatment inhibited DC differentiation in vitro. (A,B) Flow cytometry was used to evaluate the percentage of $CD11c^+$ cells (A) and $CD103^+$ cells (B) in human PBMC-derived DCs during induction with hWnt2 (30 ng/ml), hWnt2+IgG, hWnt2+αWNT2 IgG, or hWnt2+αWNT2 Fab treatment. Control: RPMI 1640 medium containing 10% FBS with GM-CSF (10 ng/ml) + IL-4 (10 ng/ml). (C,D) After DC induction with the indicated treatment, the cells were stimulated with LPS, and the percentage of $CD80^+CD11c^+$ cells (C) and $CD86^+CD11c^+$ cells (D) were assessed by flow cytometry. For the flow cytometry analyses (A-D), the acquired events were gated based on the strategy shown in online supplementary figure 4. Data are shown as means ± s.e.m. *p<0.05, **p<0.01, ***p<0.001, ****p<0.0001, using the Student's t-test. PBMC: peripheral blood mononuclear cell.

Supplementary figure 7 Detection of WNT2 expression or secretion in mEC25 tumor cells and mCAFs. (A) Western blotting showed WNT2 is more highly expressed in mCAFs than in mEC25 tumor cells. (B) ELISA assays showed WNT2 was detectable in the culture medium of mCAFs, but not in that of mEC25 cells. Data are shown as means ± s.e.m. ***p<0.001, using the Student's t-test.

Supplementary figure 8 Deregulated genes and pathways in DCs altered by mCAF-derived WNT2. (A) A Venn diagram of differentially expressed genes based on gene fold-changes ≥2.0 for three sample sets: control CM-, mCAF.CM-, or mCAF.CM+αWNT2-treated DCs; A total of 223 genes (10.6%) showed common changes in mCAF.CM-treated DCs when compared with their expression in control CM-treated DCs and mCAF CM+αWNT2-treated DCs. (B) A selection of the top nine pathways enriched for the 223 genes described in (A), based on KEGG pathway enrichment analysis.

Supplementary figure 9 p-STAT3 inhibitor Napabucasin suppressed DC differentiation. (A) Western blotting confirmed the inhibition of STAT3 (Tyr705) phosphorylation by Napabucasin (2 μM). (B,C) Napabucasin (2 μM) was used to treat cells during DC induction. Flow cytometry showed that Napabucasin suppressed the differentiation of $CD11c^+$ DCs (B) and $CD103^+$ DCs (C). (D-F) After DC induction with the indicated treatment, the cells were stimulated with LPS, and the percentage of $IL12^+CD11c^+$ cells (D), $CD80^+CD11c^+$ cells (E), and $CD86^+CD11c^+$ cells (F) were assessed by flow cytometry. Data are shown as means ± s.e.m. ***p<0.001, ****p<0.0001, using the Student's t-test.

SUPPLEMENTAL TABLES

Supplemental Table 1: siRNA sequences targeting *Socs3* and shRNA sequences targeting *Wnt2*.

Name	Sequence
si-Control	Sense: 5'-UUCUCCGAACGUGUCACGUTT-3'
	Antisense:5'-ACGUGACACGUUCGGAGAATT-3'
si-Socs3	Sense: 5'-GCUUCGACUGUGUACUCAATT-3'
	Antisense:5'-UUGAGUACACAGUCGAAGCTT-3'
shNTC	CCGGCAACAAGATGAAGAGCACCAACTCGAGTTGGTGCTCTTCATCTTGT
	TGTTTTT
shWnt2	CCGGGATGACCAAGTGTGAGTGTAACTCGAGTTACACTCACACTTGGTCA
	TCTTTTTG

SUPPLEMENTAL REFERENCES

1. Huang T, Yang J, Liu B*, et al.* A new mouse esophageal cancer cell line (mEC25)-derived pre-clinical syngeneic tumor model for immunotherapy. *Cancer Commun (Lond)* 2020;40(7):316-320.

2. Zhang C, Fu L, Fu J*, et al.* Fibroblast growth factor receptor 2-positive fibroblasts provide a suitable microenvironment for tumor development and progression in esophageal carcinoma. *Clin Cancer Res* 2009;15(12):4017-27.

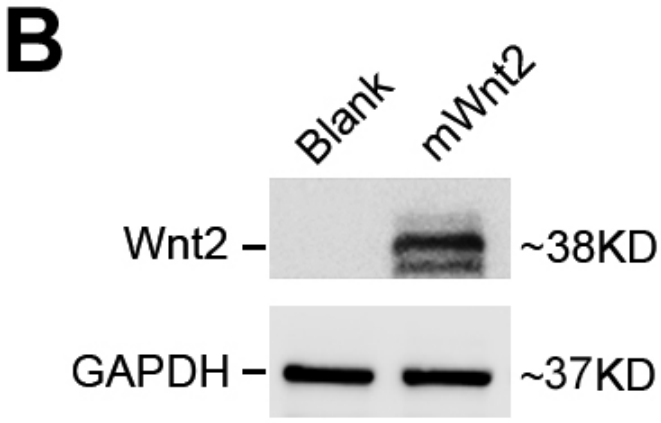

Huang et al Supplemental Figure 1

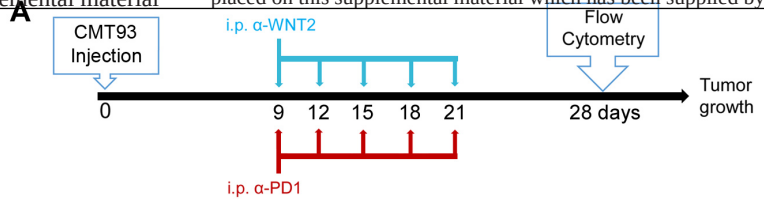

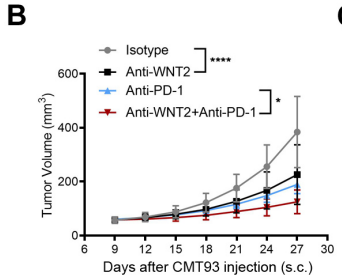

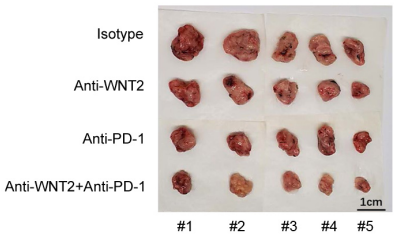

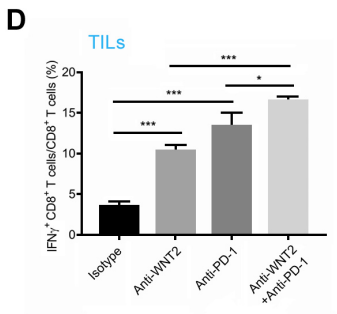

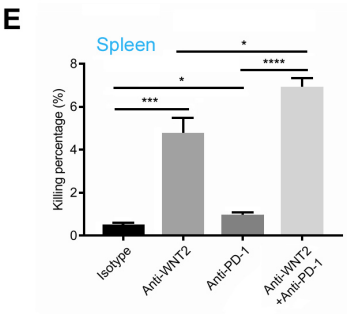

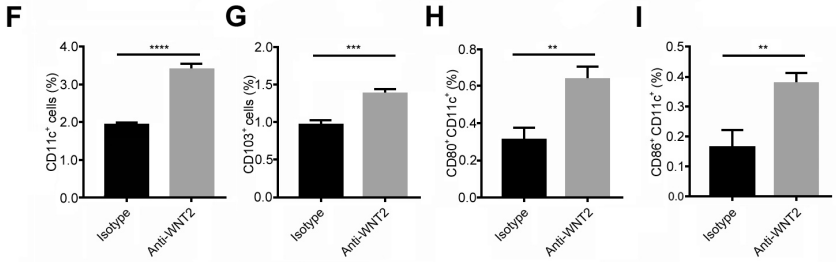

Huang et al Supplemental Figure 2

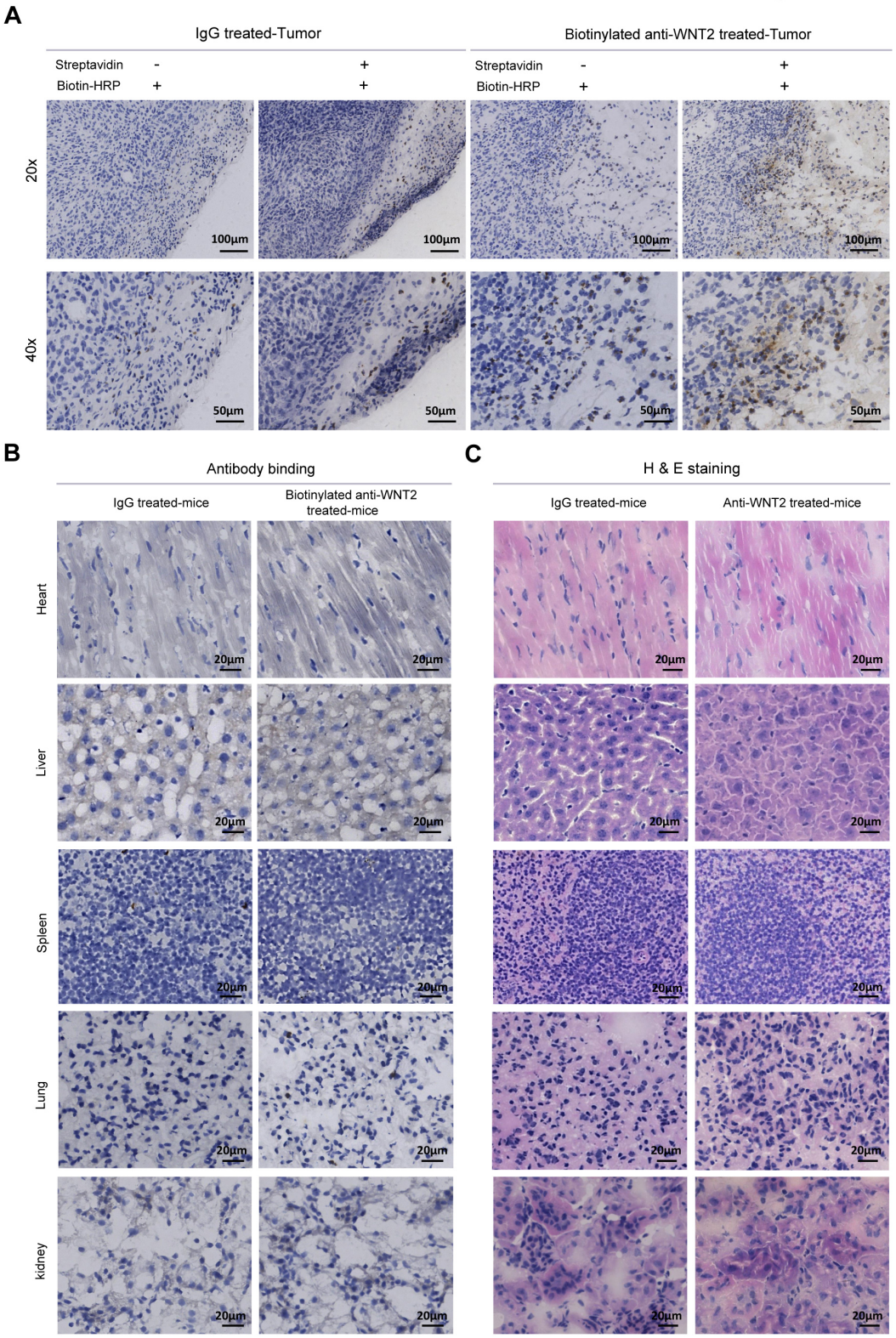

Huang et al Supplementary Figure 3

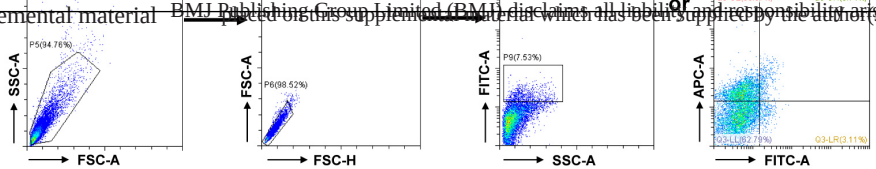

Huang et al Supplementary Figure 4

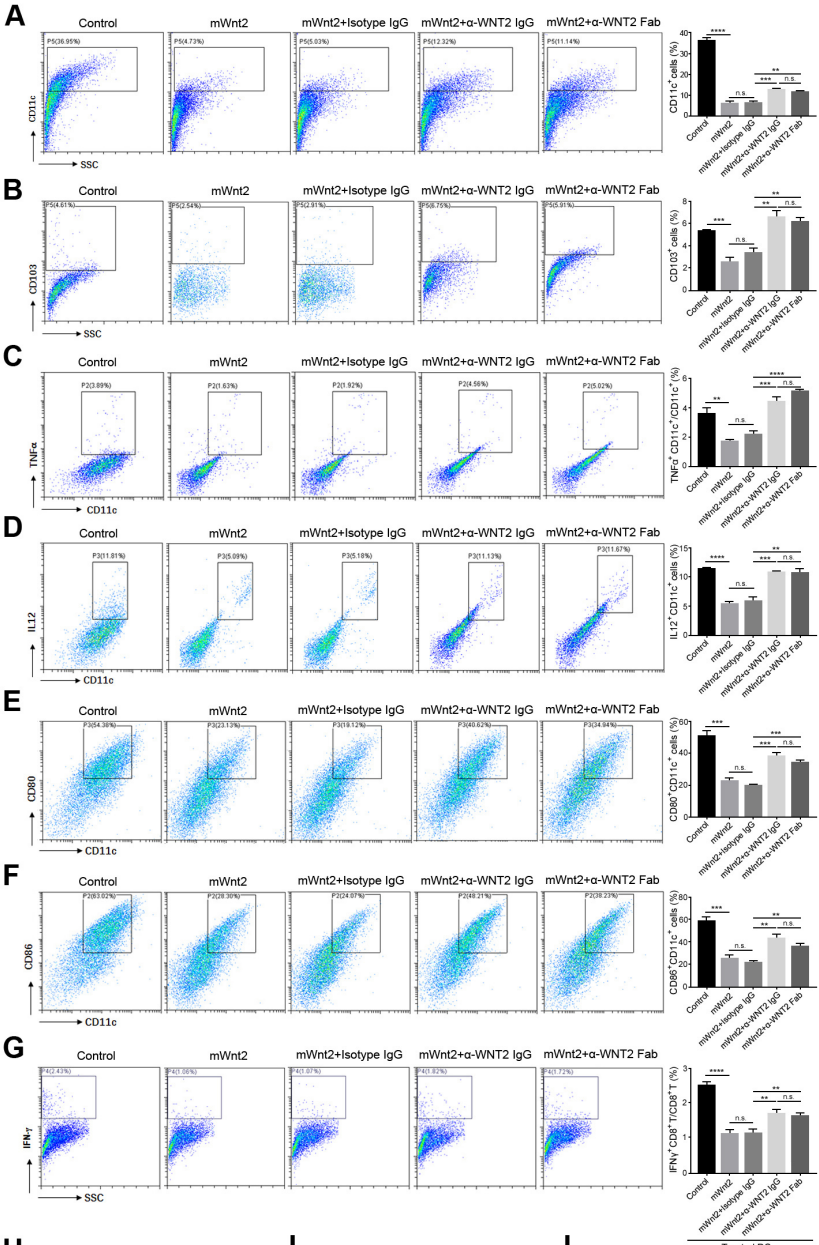

Huang et al Supplemental Figure 5

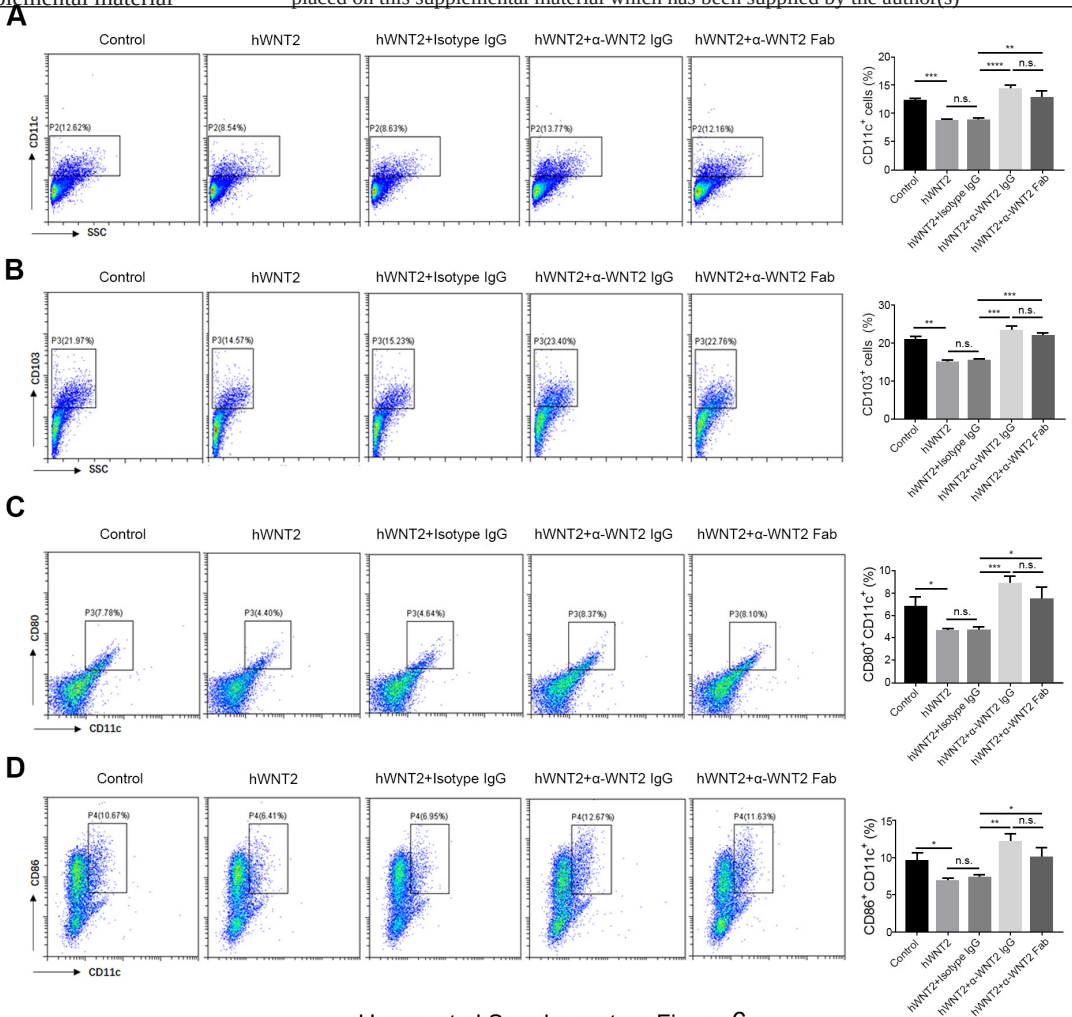

Huang et al Supplementary Figure 6

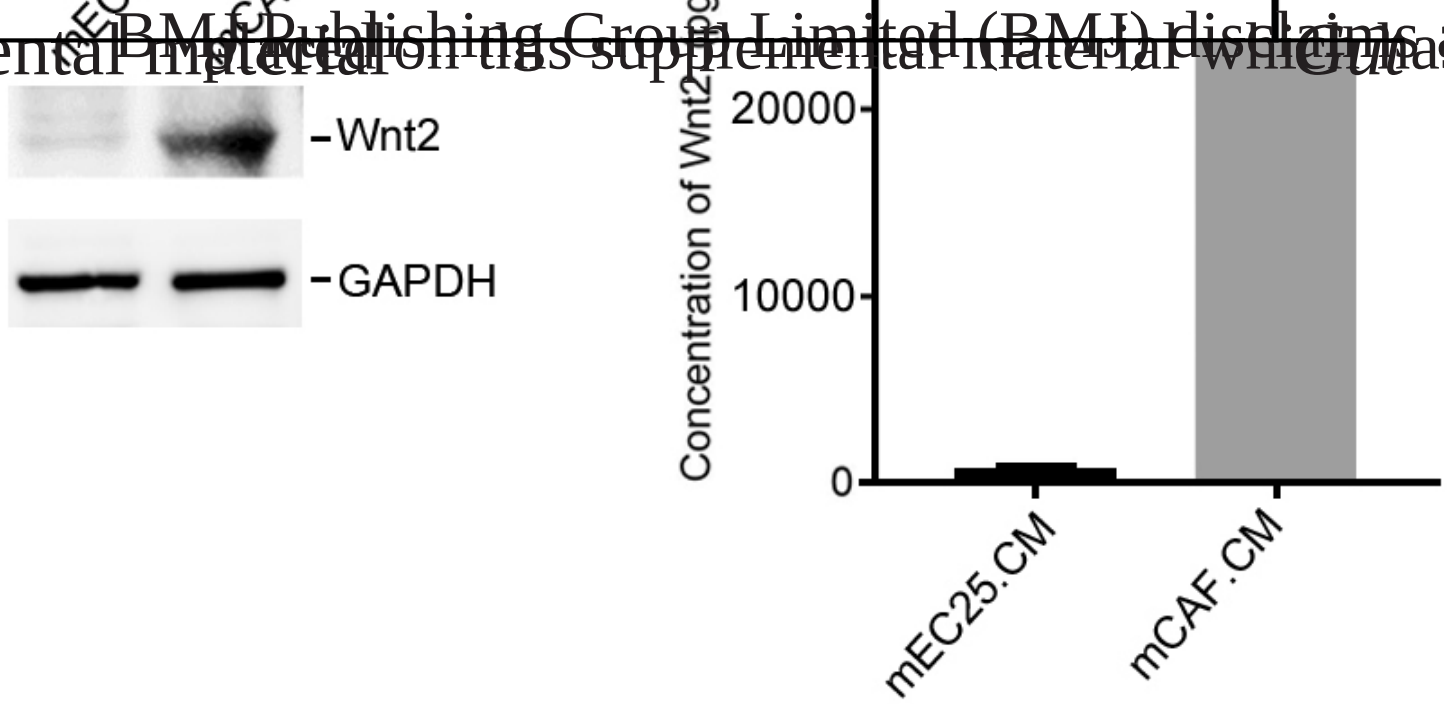

Huang et al Supplemental Figure 7

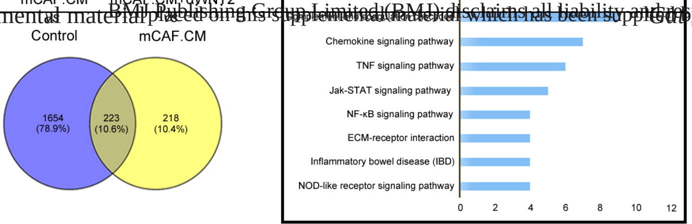

Huang et al Supplemental Figure 8

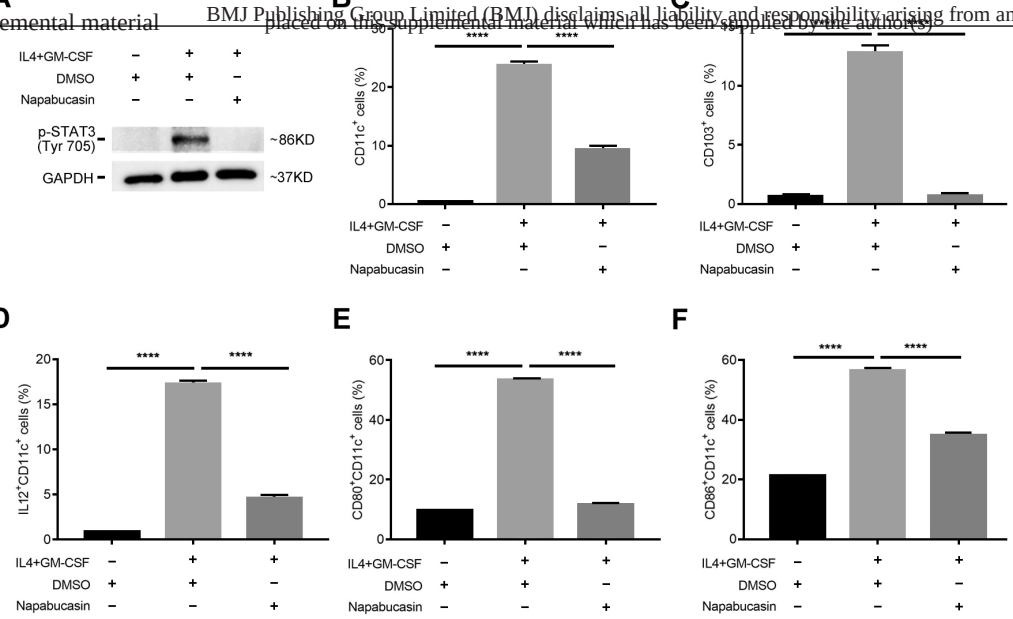

Huang et al Supplemental Figure 9

Targeting cancer-associated fibroblast-secreted WNT2 restores dendritic cell-mediated anti-tumor immunity

Tu-Xiong Huang,[1,2] Xiang-Yu Tan,[1] Hui-Si Huang,[1] Yu-Ting Li,[1] Bei-Lei Liu,[3] Kai-Sheng Liu,[2] Xin-Chun Chen,[1] Zhe Chen,[4] Xin-Yuan Guan,[3] Chang Zou,[2] Li Fu[1*]

[1]Guangdong Provincial Key Laboratory of Regional Immunity and Diseases, Department of Pharmacology and Shenzhen University International Cancer Center, Shenzhen University Health Science Center, Shenzhen 518060, Guangdong, P. R. China;

[2]Shenzhen People's Hospital (The Second Clinical Medical College, Jinan University; The First Affiliated Hospital, Southern University of Science and Technology), Shenzhen 518020, Guangdong, China;

[3]Department of Clinical Oncology, The University of Hong Kong, Hong Kong;

[4]Key Laboratory of Digestive Pathophysiology of Zhejiang Province, First Affiliated Hospital, Zhejiang Chinese Medical University, Hangzhou, 310053, China.

*Correspondence to

Dr Li Fu, Department of Pharmacology and Shenzhen University International Cancer Center, Shenzhen University Health Science Center, Shenzhen 518060, China; gracelfu@szu.edu.cn

Huang T-X, *et al. Gut* 2021;0:1–12. doi: 10.1136/gutjnl-2020-322924

SUPPLEMENTAL MATERIALS AND METHODS

Double immunofluorescence (IF)

The FFPE archived ESCC tissue sections were deparaffinized and treated with 10 mM citrate buffer (pH 6.0) at 95–100 °C for 15 min. After washing three times with phosphate-buffered saline (PBS; Gibco), the slides were treated with 0.25% Triton X-100 for 10 min and then blocked in 10% bovine serum albumin (BSA) in PBS for 1 h. A mixture of two primary antibodies (rabbit against WNT2 and mouse against FGFR2; rabbit against CD4 and mouse against FOXP3; rabbit against CD8 and mouse against IFN-γ; Abcam) was incubated overnight at 4 °C. Following washing, the slides were incubated for 1 h at room temperature with a mixture of two secondary antibodies (Alexa Fluor594-conjugated anti-rabbit IgG and Alexa Fluor488-conjugated anti-mouse IgG, or Alexa Fluor488-conjugated anti-rabbit IgG and Alexa Fluor594-conjugated anti-mouse IgG; Invitrogen) and Hoechst 33342 (Invitrogen) counterstain. Slides were subsequently mounted with ProLong™ Diamond Antifade Mountant (Invitrogen). Images were acquired using the Tissue FAXS Systems (TissueGnostics) and analyzed with TissueFAXS Imaging Software.

Clinical samples and cell lines

A total of 47 formalin-fixed and paraffin-embedded (FFPE) ESCC tissues were collected from the Shenzhen People's Hospital. All clinical samples used in this study were approved by the Committee for Ethical Review of Research at Shenzhen People's Hospital. The mouse ESCC cell line, mEC25, was established in our laboratory.[1] CMT93 mouse CRC cell line and 293T cell line were obtained from

the American Type Culture Collection. All cell lines were cultured in high-glucose DMEM (Gibco) supplemented with 10% fetal bovine serum (FBS; Gibco) and incubated at 37 °C in a humidified chamber containing 5% CO_2.

Generation of anti-WNT2 and anti-WNT2 Fab antibodies

The mouse monoclonal anti-WNT2 (3C4), which was custom-made at Kexing Biotech Inc (Hangzhou, China), is a IgG1 type antibody against human and mouse WNT2 protein. Anti-WNT2 Fab was generated based on anti-WNT2 IgG (3C4) by removing Fc fragment with enzymatic digestion methods.

Isolation of primary mouse CAFs (mCAFs)

mCAFs were isolated from mouse primary ESCC tumors that had been induced by the carcinogen 4-nitroquinoline-1-oxide (4-NQO), as previously described.[1 2] Briefly, freshly collected mouse ESCC tumor tissue was cut into pieces that were as small as possible in sterile PBS solution, followed by digestion with collagenase IV (1 mg/ml; Sigma). The suspension was filtered through the membrane of a 70-μm cell-strainer to collect a suspension of single cells. The filtrate was centrifuged, washed twice, then plated on 60-mm tissue culture dishes in 5 ml DMEM medium containing 10% FBS. After culturing for 45 min at 37 °C, non-adherent cells (mainly tumor cells) were removed to obtain pure fibroblasts. Non-tumorous esophageal tissues were used to isolate normal fibroblasts (NFs), as described above.

Lentivirus vector preparation and primary cell transduction

Lentivirus was generated with a packaging mix (Sigma) and pLKO.1-Puro-shWnt2 plasmid (Sigma) or pLKO.1-Puro-shNTC control plasmid (Sigma), according to the manufacturer's protocol. Primary mCAFs were transduced by shWnt2 of shNTC lentivirus. Puromycin (Sigma) was used to select mCAF-shWnt2 or mCAF-shNTC stable clones. The sequences for the *Socs3*-targeted siRNA and control siRNA were designed and synthesized by GenePharma (Suzhou, China); these sequences are shown in online supplementary table 1. siRNAs were transfected into primary DC precursors with Lipofectamine 3000 (Invitrogen).

Cytotoxic T lymphocyte (CTL) assay

$CD8^+$ T cells were isolated from spleens of C57BL/6 mice, using a negative $CD8^+$ T-cell isolation kit (Stemcell Technologies) and following the manufacturer's instructions. These effector $CD8^+$ T cells were re-stimulated with tumor lysate for 3 days and were then tested for cytolytic activity against mEC25 cells or CMT93 cells (effector cells : target cells = 50 : 1) using a cytotoxicity detection kit (LDH) (Roche Applied Science, Indianapolis, IN, USA), according to the manufacturer's instructions.

RNA extraction and quantitative real-time PCR

Total RNA from mCAFs or DC precursors was extracted using TRIzol Reagent (Invitrogen) and reversed-transcribed with PrimeScript™ RT-PCR Kit (Takara). Real-time PCR for analyzing Wnt2 or SOCS3 mRNA levels was performed with TB Green® Premix Ex Taq™ (Takara), according to the manufacturer's instructions, on a CFX Connect Real-Time PCR Detection System (Bio-Rad). Data

were normalized by the level of GAPDH mRNA in each individual sample. The $2^{-\Delta\Delta Ct}$ method was used to calculate relative changes in expression.

Western blotting

Western blotting was performed according to the standard protocol, using antibodies for SOCS3 (Abcam), JAK2 (D2E12; CST), p-JAK2 (D15E2; CST), STAT3 (79D7; CST), p-STAT3 Tyr705 (D3A7; CST), or GAPDH (D16H11; CST), and then with HRP-conjugated secondary antibody after washing. The bands on the membranes were detected using a Pierce™ Fast Western Blot Kit (Thermo Scientific) and the ChemiDoc Touch Gel Imaging system (Bio-Rad).

RNA sequence analysis

Total RNA from control CM, mWnt2, mCAF.CM, or mCAF.CM+αWNT2 treated DCs was depleted of genomic DNA and rRNA. After purification of the remaining RNA without rRNA, the RNA was fragmented into small pieces using divalent cations under elevated temperature. The cleaved RNA fragments were copied into first strand cDNA using reverse transcriptase and random primers, followed by second strand cDNA synthesis. These cDNA fragments then were subjected to end-repair, phosphorylation and 'A' base addition according to Illumina library construction protocol. Deep sequencing was performed on an Illumina NovaSeq 6000 at WuXi NextCODE (Shanghai, China). RSEM (1.2.29) were used to perform expression abundance quantification based on the uniquely mapped reads. Transcripts with fold change ≥ 2 in expression level were defined as differentially

expressed. Hypergeometric test implemented in GOSTATs was used to perform functional enrichment analysis and gene set enrichment analysis. The RNA-sequencing data generated in this investigation were deposited in the National Center for Biotechnology Information's Gene Expression Omnibus (GEO) database and can be accessed using GEO accession no. GSE154420.

ELISA analysis

Cell culture supernatants of mCAF-shWnt2 or mCAF-shNTC clones were collected, and the concentration of Wnt2 was measured using the mouse Wnt2 ELISA kit (CUSABIO), according to the manufacturer's instructions. For detecting the secretion of TNFα and IL12 by DCs as well as the secretion of IFNγ by $CD8^+$ T cells, the cells were treated as in FACS assay followed by the collection of their culture-supernatant. The concentration of TNFα, IL12, or IFNγ in the culture-supernatant was detected using the corresponding ELISA kit (Biolegend).

Immunohistochemical (IHC) and hematoxylin/eosin (HE) analysis

Isotype IgG or biotin-labeled anti-WNT2 was injected into mEC25-tumor bearing C57BL/6 mice intraperitoneally every two days for three times, and the tumors and normal organs including heart, liver, spleen, lung, and kidney were isolated. Consecutive frozen sections and streptavidin-biotin-HRP complex method were used for IHC analysis. In brief, frozen tissue sections were blocked with 0.3% hydrogen peroxide for 15min, and with 10% normal rabbit serum for 10min, followed by the incubation of streptavidin-biotin-HRP complex. Streptavidin was omitted as the negative staining control. The

slides were visualized using 3, 3'-diaminobenzidine (Dako), and then counterstained with hematoxylin (Sigma-Aldrich). For the histological analyses, consecutive human ESCC tissue sections used for the IF analyses of WNT2$^+$ CAFs, Tregs, and effector CD8$^+$ T cells, or the frozen sections of normal organs from the mice in IgG and anti-WNT2 treatment group, were stained with HE according to the manufacturer's instructions (Vector, Burlingame, CA). The images were captured with Slide Scan System (SQS1000; TEKSQRAY).

Statistical analysis

All quantitative data are presented as means ± standard error of the mean (s.e.m.), unless otherwise indicated. The statistical analyses were performed using an unpaired two-tailed Student's *t*-test or two-way ANOVA, using the Prism statistical software program (GraphPad Software, Inc., San Diego, CA, USA). A P-value less than 0.05 was considered to be significant. *P<0.05, **P<0.01, ***P<0.001,****P<0.0001.

SUPPLEMENTAL FIGURE LEGENDS

Supplementary figure 1 Identification of the specificity and species reactivity of the anti-WNT2 monoclonal antibody. (A) Western blotting revealed that anti-WNT2 monoclonal antibody (Clone: 3C4) specifically recognized the cell lysate of 293T cells with overexpression of human WNT2, but not those with overexpression of human WNT2B, WNT3A, WNT5A, WNT5B, WNT7B, or WNT11. GAPDH was used as an internal control. (B) Western blotting revealed that anti-WNT2 recognized the

cell lysate of 293T cells with mouse Wnt2 overexpression. GAPDH was used as an internal control.

Supplementary figure 2 Anti-WNT2 therapy induced tumor-killing immunity and enhanced the therapeutic efficacy of anti-PD-1 in mouse CRC. (A) Schematic of the drug intervention protocol for α-WNT2 (intraperitoneally) and/or α-PD1 (intraperitoneally) in C57BL/6 mice subcutaneously implanted with CMT93 cells. At the drug intervention end-point, mouse tissues were obtained for flow cytometry. (B) Average tumor growth curves of syngeneic CMT93 tumors in mice treated as described in (A). (C) The visual maps of CMT93 tumors by indicated treatment. The tumors were removed from mice at day 30 after CMT93 cell injection. (D) Flow cytometry was used to quantify the percentage of effective $CD8^+$ T cells ($IFN\gamma^+$) in anti-WNT2, anti-PD-1, and IgG isotype-treated mice (n=5/group). (E) A cytotoxic lymphocyte (CTL) assay evaluated the tumor-killing activity of $CD8^+$ T cells isolated from mice spleen treated in (D). (F-I) Flow cytometry analysis was used to quantify the percentage of $CD11c^+$ DC cells (F), $CD103^+$ DC cells (G), $CD80^+CD11c^+$ DC cells (H), and $CD86^+CD11c^+$ cells (I) in tumors from mice treated in (D). Data are shown as means ± s.e.m. *p<0.05, **p<0.01, ***p<0.001, ****p<0.0001 by two-way ANOVA in (B) or Student's t-test in (D-I).

Supplementary figure 3 Evaluation of the potential off target effects of anti-WNT2. (A,B) IHC analysis was used to evaluate the binding activities of biotin-labeled anti-WNT2 to tumor tissues (A) and normal vital organs including heart, liver, spleen, lung and kidney (B) after intraperitoneal injection into mice. Scale bar: 100μm (Upper panel); 50μm (Lower panel). (C) Representative H&E staining of

normal vital organs from the anti-WNT2-treated and IgG-treated mice. Scale bar: 20μm.

Supplementary figure 4 Gating strategy used for flow cytometry analyses. For the analyses of flow cytometry experiments, the acquired events were firstly gated based on the forward scatter (FSC-A) and side scatter (SSC-A) plots. Single cells were then gated based on the height and area of FSC (FSC-H vs. FSC-A) and analyzed for the indicated cell surface markers which were stained with specific fluorescence-labeled antibodies. The obtained data were processed using Beckman CytExpert software.

Supplementary figure 5 Recombinant mouse-Wnt2 protein inhibited DC differentiation in vitro. (A,B) Flow cytometry was used to evaluate the percentage of $CD11c^+$ cells (A) and $CD103^+$ cells (B) in C57BL/6 bone marrow cells during DC induction with mWnt2 (100 ng/ml), mWnt2+IgG, mWnt2+αWNT2 IgG or mWnt2+αWNT2 Fab treatment. Control: RPMI 1640 medium containing 10% FBS with GM-CSF (10 ng/ml) + IL-4 (10 ng/ml). (C-F) After DC induction with the indicated treatment, the cells were stimulated with LPS, and the percentage of $TNF\alpha^+CD11c^+$ cells (C), $IL12^+CD11c^+$ cells (D), $CD80^+CD11c^+$ cells (E) and $CD86^+CD11c^+$ cells (F) was assessed by flow cytometry. (G) After DC induction with the indicated treatment, the cells were stimulated with mEC25 cell lysate followed by co-incubation with $CD8^+$ T cells for 5 days, and the percentage of $IFN\gamma^+CD8^+$ T cells in $CD8^+$ gated cells was evaluated by flow cytometry. (H-J) ELISA assay was used to detect the secretion of TNFα (H) and IL12 (I) by DCs, and the secretion of IFNγ (J) by $CD8^+$ T cells with the

indicated treatment. For the flow cytometry analyses (A-G), the acquired events were gated based on the strategy shown in online supplementary figure 4. Data are shown as means ± s.e.m. **p<0.01, ***p<0.001, ****p<0.0001, using the Student's t-test. LPS, lipopolysaccharide.

Supplementary figure 6 Recombinant human-WNT2 protein treatment inhibited DC differentiation in vitro. (A,B) Flow cytometry was used to evaluate the percentage of $CD11c^+$ cells (A) and $CD103^+$ cells (B) in human PBMC-derived DCs during induction with hWnt2 (30 ng/ml), hWnt2+IgG, hWnt2+αWNT2 IgG, or hWnt2+αWNT2 Fab treatment. Control: RPMI 1640 medium containing 10% FBS with GM-CSF (10 ng/ml) + IL-4 (10 ng/ml). (C,D) After DC induction with the indicated treatment, the cells were stimulated with LPS, and the percentage of $CD80^+CD11c^+$ cells (C) and $CD86^+CD11c^+$ cells (D) were assessed by flow cytometry. For the flow cytometry analyses (A-D), the acquired events were gated based on the strategy shown in online supplementary figure 4. Data are shown as means ± s.e.m. *p<0.05, **p<0.01, ***p<0.001, ****p<0.0001, using the Student's t-test. PBMC: peripheral blood mononuclear cell.

Supplementary figure 7 Detection of WNT2 expression or secretion in mEC25 tumor cells and mCAFs. (A) Western blotting showed WNT2 is more highly expressed in mCAFs than in mEC25 tumor cells. (B) ELISA assays showed WNT2 was detectable in the culture medium of mCAFs, but not in that of mEC25 cells. Data are shown as means ± s.e.m. ***p<0.001, using the Student's t-test.

Supplementary figure 8 Deregulated genes and pathways in DCs altered by mCAF-derived WNT2. (A) A Venn diagram of differentially expressed genes based on gene fold-changes ≥2.0 for three sample sets: control CM-, mCAF.CM-, or mCAF.CM+αWNT2-treated DCs; A total of 223 genes (10.6%) showed common changes in mCAF.CM-treated DCs when compared with their expression in control CM-treated DCs and mCAF CM+αWNT2-treated DCs. (B) A selection of the top nine pathways enriched for the 223 genes described in (A), based on KEGG pathway enrichment analysis.

Supplementary figure 9 p-STAT3 inhibitor Napabucasin suppressed DC differentiation. (A) Western blotting confirmed the inhibition of STAT3 (Tyr705) phosphorylation by Napabucasin (2 μM). (B,C) Napabucasin (2 μM) was used to treat cells during DC induction. Flow cytometry showed that Napabucasin suppressed the differentiation of $CD11c^+$ DCs (B) and $CD103^+$ DCs (C). (D-F) After DC induction with the indicated treatment, the cells were stimulated with LPS, and the percentage of $IL12^+CD11c^+$ cells (D), $CD80^+CD11c^+$ cells (E), and $CD86^+CD11c^+$ cells (F) were assessed by flow cytometry. Data are shown as means ± s.e.m. ***p<0.001, ****p<0.0001, using the Student's t-test.

SUPPLEMENTAL TABLES

Supplemental Table 1: siRNA sequences targeting *Socs3* and shRNA sequences targeting *Wnt2*.

Name	Sequence
si-Control	Sense: 5'-UUCUCCGAACGUGUCACGUTT-3'
	Antisense:5'-ACGUGACACGUUCGGAGAATT-3'
si-Socs3	Sense: 5'-GCUUCGACUGUGUACUCAATT-3'
	Antisense:5'-UUGAGUACACAGUCGAAGCTT-3'
shNTC	CCGGCAACAAGATGAAGAGCACCAACTCGAGTTGGTGCTCTTCATCTTGT
	TGTTTTT
shWnt2	CCGGGATGACCAAGTGTGAGTGTAACTCGAGTTACACTCACACTTGGTCA
	TCTTTTTG

SUPPLEMENTAL REFERENCES

1. Huang T, Yang J, Liu B*, et al.* A new mouse esophageal cancer cell line (mEC25)-derived pre-clinical syngeneic tumor model for immunotherapy. *Cancer Commun (Lond)* 2020;40(7):316-320.

2. Zhang C, Fu L, Fu J*, et al.* Fibroblast growth factor receptor 2-positive fibroblasts provide a suitable microenvironment for tumor development and progression in esophageal carcinoma. *Clin Cancer Res* 2009;15(12):4017-27.

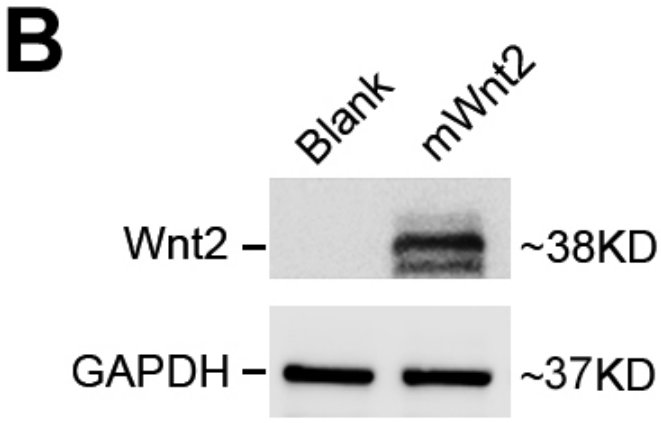

Huang et al Supplemental Figure 1

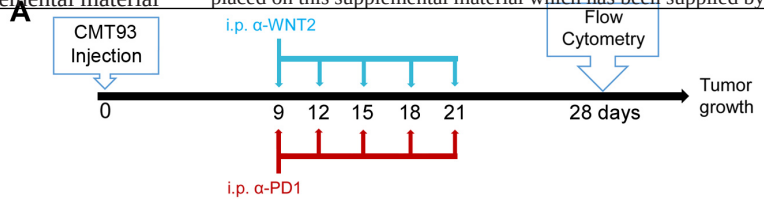

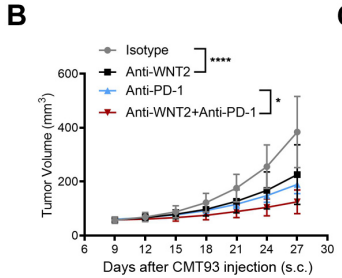

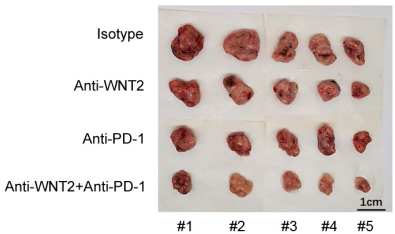

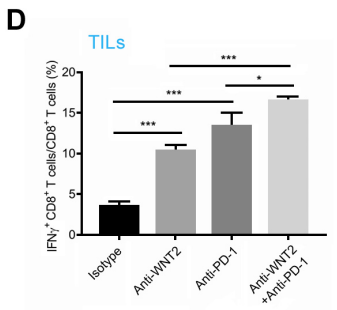

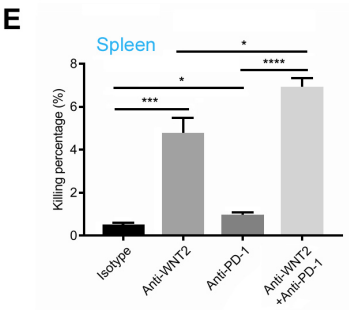

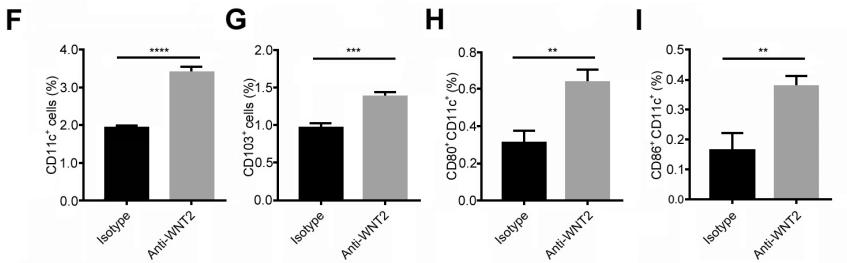

Huang et al Supplemental Figure 2

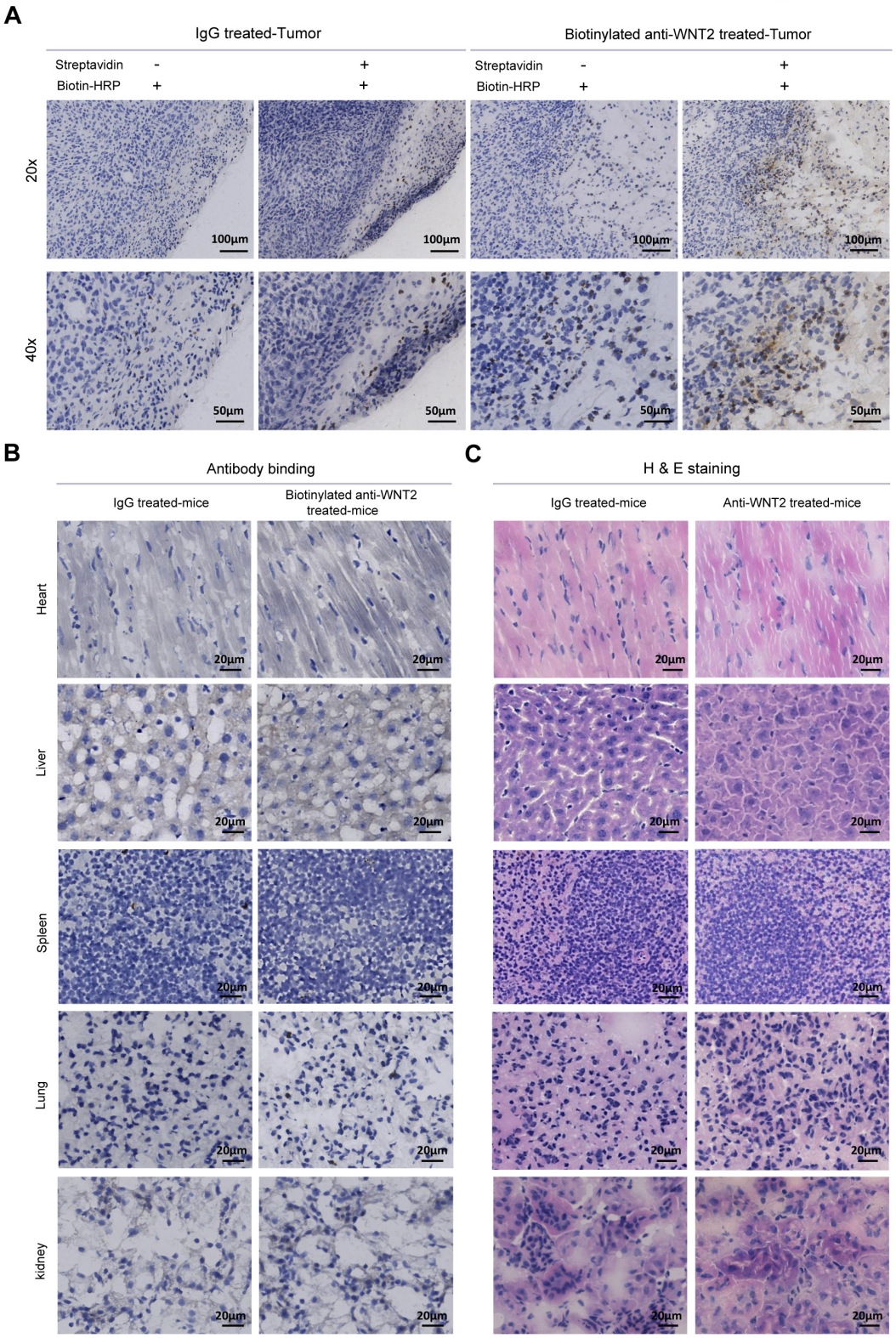

Huang et al Supplementary Figure 3

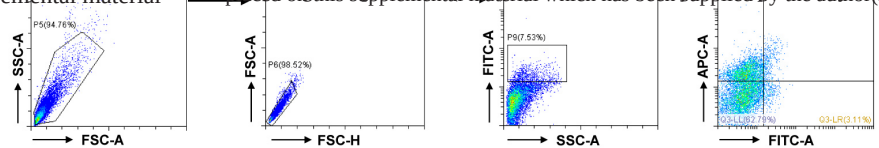

Huang et al Supplementary Figure 4

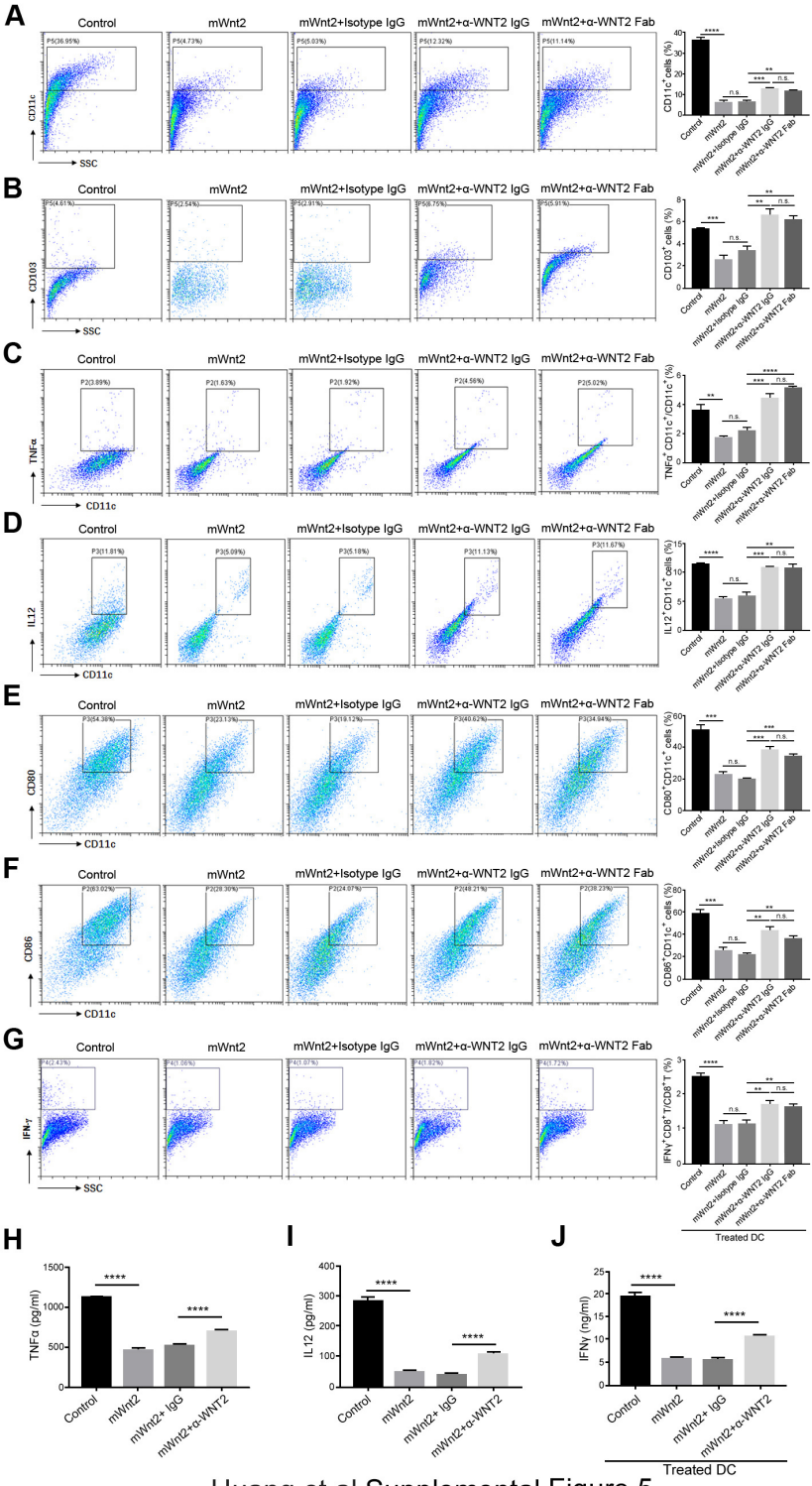

Huang et al Supplemental Figure 5

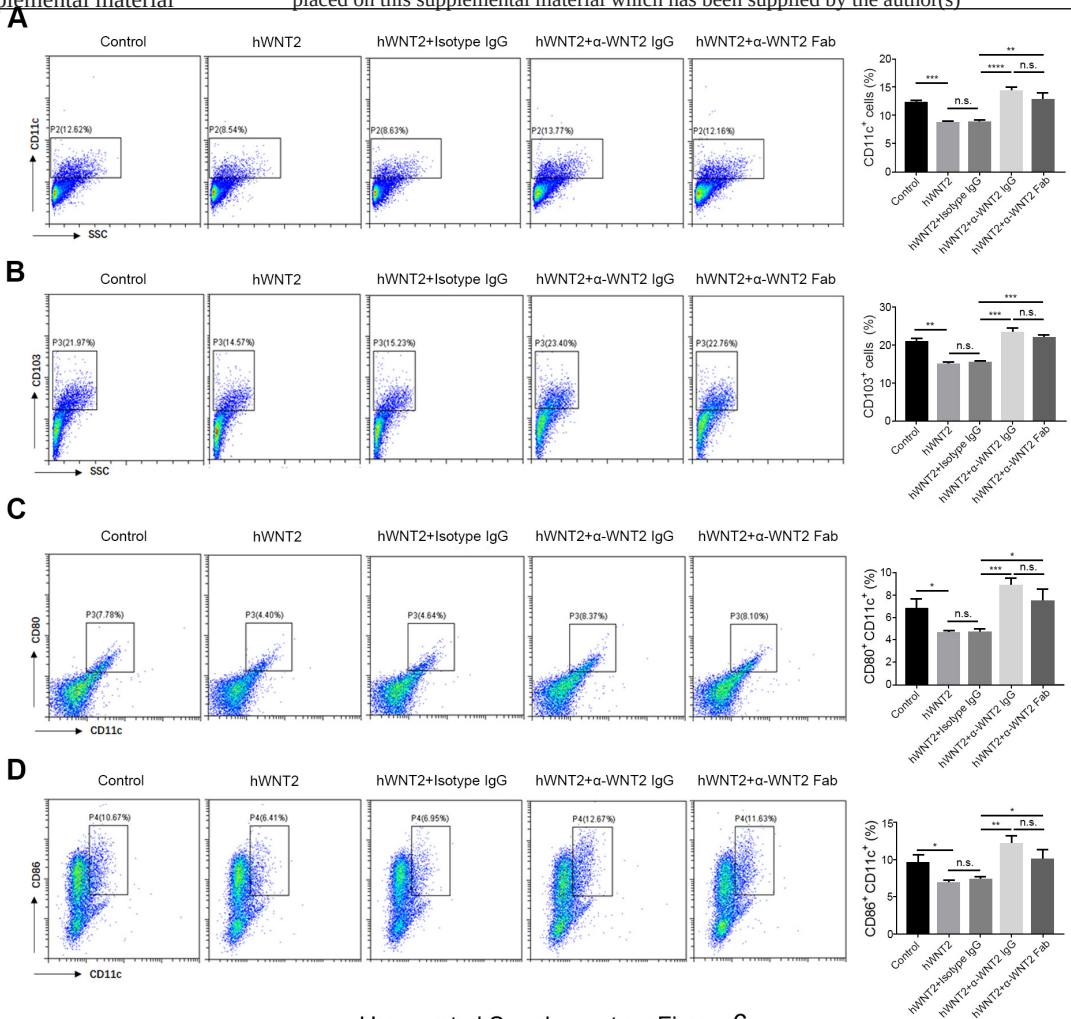

Huang et al Supplementary Figure 6

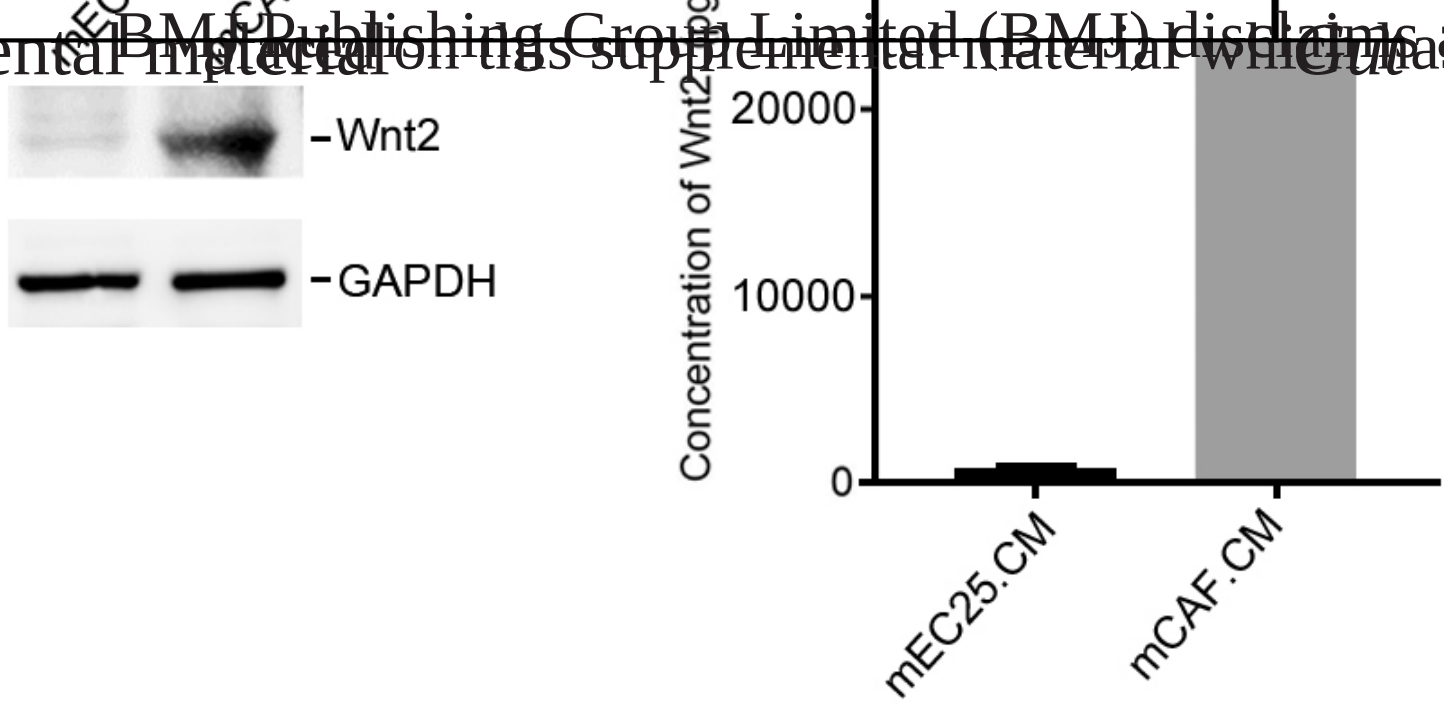

Huang et al Supplemental Figure 7

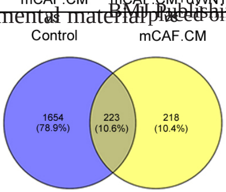

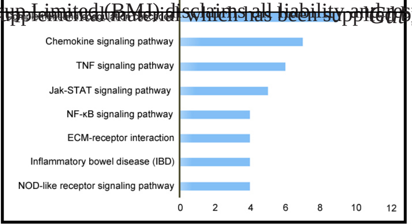

Huang et al Supplemental Figure 8

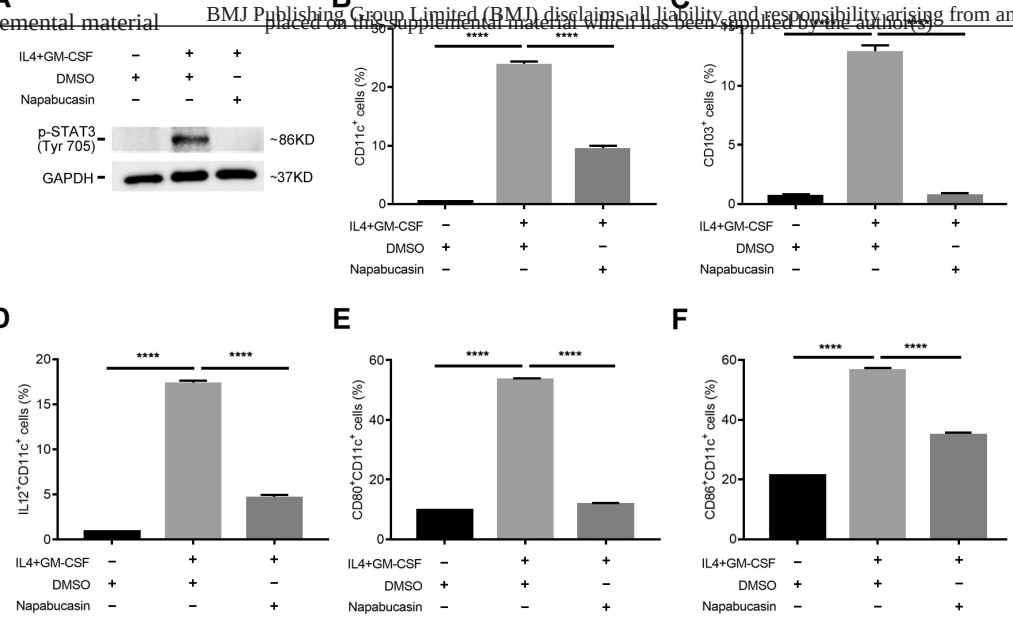

Huang et al Supplemental Figure 9